Shunt Resistor Based Circuit Breaker Design for Ground Fault and Arc Fault Detection

A Major Qualifying Project Report

March 27, 2024

By:

Pari Nguyen

Olivia Peterson

Dominic Ridolfi

Elinor Ross

Mason Roth

Project Advisors: Edvina Uzunovic and Reinhold Ludwig

Sponsor Representatives: Paul Reid and Christopher Mello

Sponsored By:

Abstract

Under the guidance of Schneider Electric, this Major Qualifying Project aimed to replace traditional inductive coils in ground fault and arc fault circuit interrupters. The project sought to utilize resistive shunts or other sensing components for fault detection. The team designed, simulated, and constructed a successful prototype that employed metal film shunt resistors for ground fault detection and a ferrite bead serving as an inline inductor for arc fault detection. Additional consideration was given to the thermal behavior of the sensing components using an infrared camera. Testing demonstrated that a thermal differential between components will not cause erroneous tripping of the breaker.

Acknowledgements

The team would like to extend our sincerest gratitude to our sponsor company, Schneider Electric, for generously providing support to this MQP. We would specifically like to thank their representatives, Paul Reid and Christopher Mello, for providing ongoing guidance and expertise throughout this project. We would like to thank our advisors, Professor Edvina Uzunovic and Professor Reinhold Ludwig whose assistance, direction, and feedback made this project possible. Finally, we would like to thank electronic technician Bill Appleyard from the Atwater Kent ECE shop for ordering our materials and providing access to his shop and equipment.

Executive Summary

Current methods of ground fault and arc fault detection utilize inductive coils to detect voltage changes for ground faults, series arc faults, and parallel arc faults. These coils are proportionally large, relatively expensive, and can erroneously trip due to non-standard electrical noise. This MQP explores alternatives to using inductive coils for fault detection.

The objective of this project was to create a ground fault and arc fault circuit interrupter device in which the inductive coil is replaced by a set of resistive shunts or other series components to provide both ground fault and arc fault sensing. As specified by the sponsor, the ground fault circuit interrupter (GFCI) device needed to detect a 5mA ground fault current in the presence of a 20A load current and the arc fault circuit interrupter (AFCI) device needed to detect a 100μA signal in a frequency range of 10-20MHz. Testing was first performed with a 12VAC/3.33A source and then a 24VAC/20A source.

The GFCI circuit consists of two metal film shunt resistors, one on the live line and one on the neutral line. Each shunt has a differential amplifier measuring the voltage across it. This signal is filtered and amplified for microcontroller signal processing. The microcontroller detects a fault by calculating the differential voltages across the shunts. When a ground fault occurs, the voltage across the shunt on the neutral line decreases, decreasing differential voltage.

The sensing component for the AFCI device is a ferrite bead on the live line. At the 60Hz operating frequency, the power loss of the ferrite bead is negligible. When a high frequency signal is passed through it, resistance increases, causing a voltage drop. A microcontroller reads the voltage drop across the bead to determine when a high frequency signal is being injected.

Both the GFCI and AFCI devices were able to detect their respective faults, proving that the proposed design can serve as a replacement for the traditional breaker design. Limitations of the prototype include delayed response time for tripping, compatibility only with purely resistive loads, and the absence of a tripping mechanism.

Table of Contents

Authorship Table

Section	Author(s)
Abstract	E.R.
Acknowledgements	E.R.
Executive Summary	E.R.
1. Introduction	D.R.
2.1 Need for Ground Fault and Arc Fault Circuit Interrupters	E.R.
2.2 Current Solutions	E.R.
3. Problem Statement and Objectives	E.R.
4. Design Approach	E.R. O.P.
4.1 Source and Load	E.R. O.P.
4.2 Resistive Shunts	E.R.
4.3 Amplification and Filtering for Ground Fault Circuit Interrupter	O.P.
4.4 Ground Fault Circuit Interrupter Signal Processing	M.R.
4.5 High Frequency Signal Injection	D.R. P.N.
4.6 Arc Fault Circuit Interrupter Inductive Element Selection	D.R. P.N.
4.7 Inductor Testing and Filter Design for Arc Fault Circuit Interrupter	D.R. P.N.
4.8 Arc Fault Circuit Interrupter Signal Processing	M.R.
4.9 Higher Power Modifications	D.R. M.R. O.P.
5.1 Ground Fault Circuit Interrupter Schematic and Simulations	E.R.
5.2 Arc Fault Circuit Interrupter Schematic and Simulations	D.R. P.N.
5.3 Combined Dual Function Breaker Schematic and Simulations	O.P. P.N.
6.1 Higher Power Testing Results	All
6.2 Thermal Testing	E.R. M.R. O.P.
7.1 Meeting Objectives	All
7.2 Limitations	All
7.3 Safety and Environmental Impact	O.P.
7.4 Manufacturability	E.R. M.R.
9. Conclusion	O.P.
8.1 120V Research	E.R.
8.2 Microcontroller Improvement	D.R.
8.3 Creating a Printed Circuit Board	O.P.
Appendix A. Abbreviations	M.R. O.P.
Appendix B. LTspice GFCI Schematic and Simulation	O.P.
Appendix C. Ground Fault Detection Arduino Code	M.R.
Appendix D. Arc Fault Detection Arduino Code	M.R.

Table of Figures

Table of Tables

1. Introduction

Electrical safety is vital when transmitting electric power to residential, industrial, or commercial sectors. Electrical transmission and distribution have the inherent risk of faults occurring, leading to potential fires, property damage, and human injuries, even death. To mitigate these dangers, ground fault and arc fault detectors have been employed in circuit breakers. Current methods of fault detection, among other methods, utilize proportionally large inductive coils to detect voltage changes for ground faults, series arc faults, and parallel arc faults [1]. Figure 1 shows a Schneider Electric dual function ground fault and arc fault circuit interrupter with the sensing transformer labeled. These transformers are large, relatively expensive, and can erroneously trip due to non-standard electrical noise [2]. For these reasons, circuit breaker designers have been researching alternatives to using inductive coils for fault detection.

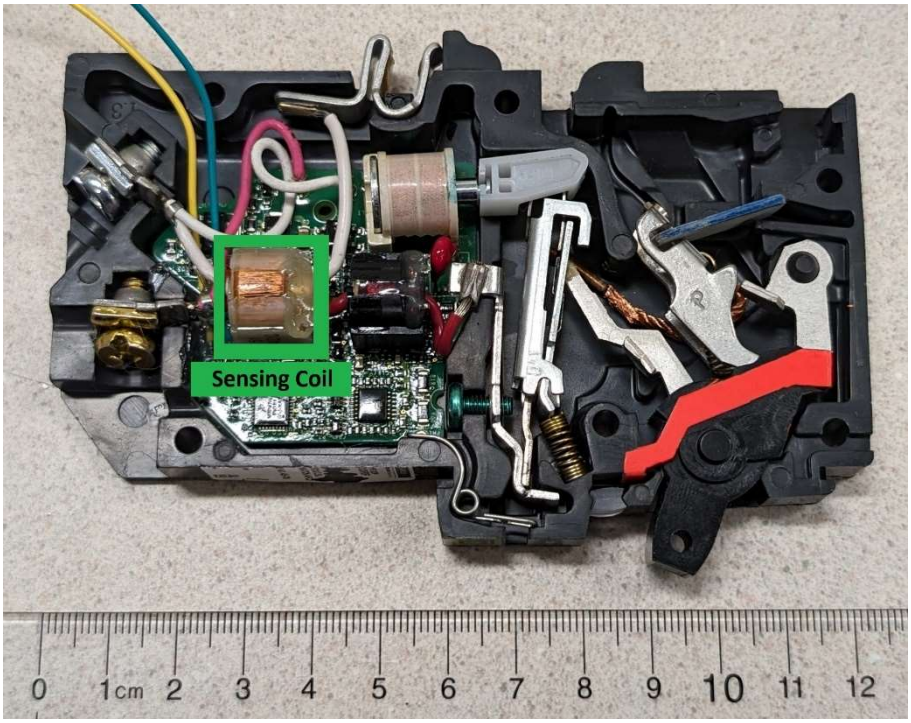

Figure 1. A Schneider Electric dual function breaker with sensing transformer.

Incorporation of dual shunt resistance for fault detection could improve size, safety, and efficacy of the current transformer-based design. Measuring and comparing the voltage drop over the shunt resistances allows the ratio of the shunts to mitigate standard noise and sense poor quality power. By utilizing passive components that provide insight to the electrical behavior of the

electrical circuit, the breaker's sensing system also provides real-time monitoring and detection of fault characteristics, allowing for a quick response and increased electrical safety.

2. Background

2.1 Need for Ground and Arc Fault Circuit Interrupters

To understand the need for ground and arc fault circuit interrupters, it is critical to understand what faults are and why they are dangerous. Ground faults occur when electrical current unintentionally flows in a path from a conductor to ground as seen in Figure 2. This results in less current passing through the load [3]. Ground faults commonly occur when there is damage to insulation around the conductor or excess moisture surrounding it. When the ground fault current path is through equipment, the high fault current can cause electrical damage or fires. In the extreme case, when the path is through a living being, there is risk of electrocution [1].

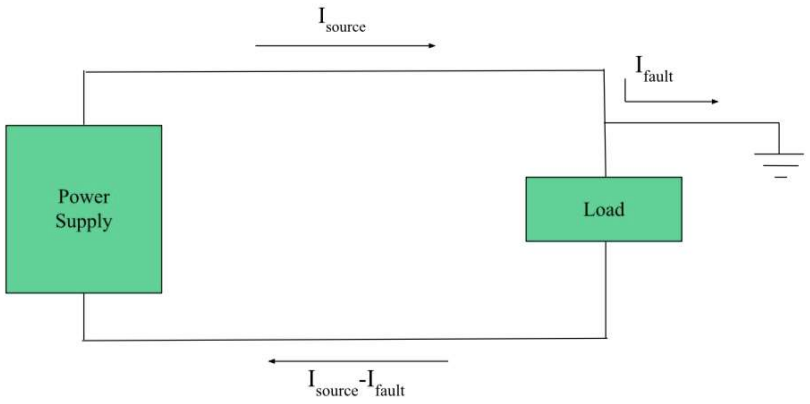

Figure 2. Unintentional path to ground causing a ground fault.

Arc faults occur when there is an unintended arcing or sparking of electricity across a gap within a conductor, as seen in Figure 3. Arc faults can be either a series arc or a parallel arc. In a series arc, current is transferred across a broken wire or conductor. In a parallel arc, current is transferred across multiple conductors, usually resulting from damaged insulation [4]. Arc faults pose a serious fire hazard, as the arcing current can heat up and can ignite surrounding materials [5]. Arc faults are typically detectable due to the high frequency noise that occurs in both the voltage and current signals of the connected circuit [6].

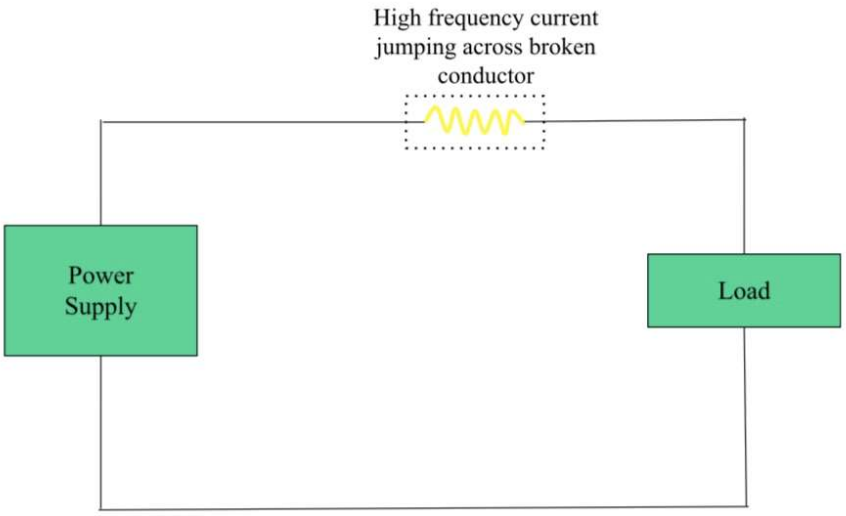

Figure 3. Series arc fault across a broken conductor.

2.2 Current Solutions

The Schneider Electric company began manufacturing residential circuit breakers in 1935 to protect lighting circuits from current overloads and short circuits [7]. Ground fault and arc fault circuit interruption were incorporated into the design of residential circuit breakers in 1971 and 1994, respectively [8]. Since then, these devices have proved to be successful in interrupting faults and protecting humans and property from electrical damage.

The most popular design approach for ground fault circuit interrupters (GFCIs) uses a transformer to compare current to and from the load. When a ground fault occurs, it disrupts the balance in the transformer, leading to the generation of a low voltage signal. The voltage signal is amplified and analyzed by a logic circuit or microcontroller, which then instructs the breaker to trip and interrupt the current flow into the load [1].

The traditional arc fault circuit interrupter (AFCI) design uses a transformer to detect the current flow from the load. The signal is subsequently passed through a band-pass filter designed to pass high frequency arc waveform components. The center frequency of the band-pass filter determines which arcing frequencies the circuit will interrupt. A microcontroller uses this high frequency information along with analysis of the line frequency current to determine if the arc can cause various hazards including fire, electrical damage, or electrocution. If it is determined to be hazardous, a signal is sent to the circuit breaker to interrupt the current into the load [9]. The

microcontroller must be programmed to detect the voltage for ground faults and distinguish chaotic characteristics of unacceptable arcs.

Figure 4 shows the typical design for a dual function GFCI/AFCI circuit breaker. The thermal sensor in a standard pole dual function circuit breaker is for detecting an over current that is slightly above the rating of the circuit breaker. This is achieved with the use of a bimetallic element that expands as it is heated due to its resistive nature. When this bimetallic element expands, its movement causes the circuit breaker to trip [10]. The magnetic sensor is an electromagnet that causes the breaker to trip if the current is significantly over the current rating of the breaker. When a high current passes through the magnetic sensor element of the breaker, the induced magnetic flux triggers the breaker to trip and open the circuit [11].

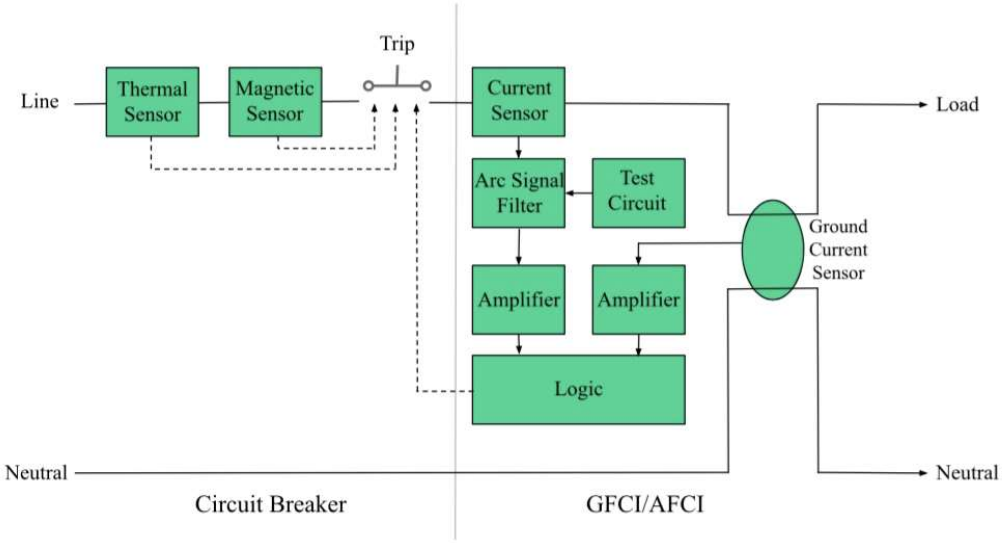

Figure 4. Pole dual function circuit breaker block diagram [9].

3. Problem Statement and Objectives

The objective of this project was to create a combined GFCI and AFCI device in which the inductive coil is replaced by a set of resistive shunts or other series components that provide both ground fault and arc fault sensing. The block diagram in Figure 5 was provided by the Major Qualifying Project sponsor, Schneider Electric, as an initial design concept.

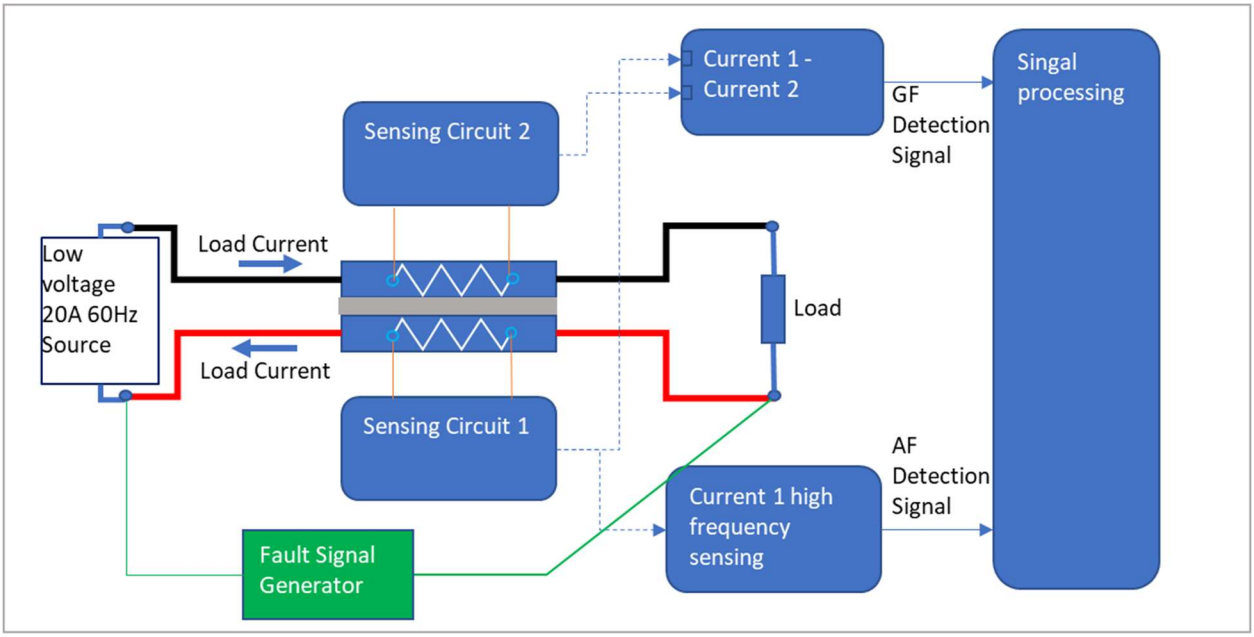

Figure 5. Dual shunt GFCI/AFCI circuit block diagram.

As specified by the sponsor, the GFCI device must sense a 5mA ground fault current in the presence of a 20A load current, which means the fault current is 0.025% of the total load current. This specification corresponds to UL Standard 943 which states that "a Class A ground-fault circuit-interrupter shall be capable of interrupting the electric circuit to the load when the fault current to ground is within the range of a minimum of 6mA through a maximum of (110% of rated V/500) mA. Interruption of the electric circuit to the load shall not take place if the fault current is less than 4mA" [12].

At the advice of Schneider Electric, the team decided to first design a proof-of-concept prototype to sense a 5mA ground fault current from a 3.33A load current. In this case, the fault current is 1.5% of the load current. In addition to a more easily detectable fault current, the low power prototype provided safer testing conditions.

The overall GFCI problem statement was broken into a series of smaller objectives. First, the team needed to evaluate resistive materials with very low or predictable temperature coefficients to reduce thermal drift of the shunts. From there, the voltage across each shunt needed to be measured while maintaining electrical isolation between shunts. Finally, the team needed to find the difference between the voltage measured across each shunt. Under normal conditions, the voltage measured across each shunt should be identical since the same amount of current is flowing

on the live and neutral lines. If there is a fault occurring, the currents on the live and neutral lines would no longer be equal and, therefore, the voltage drops across the shunts would differ. In addition to these objectives provided by the sponsor, the team included an additional goal to follow UL Standard 943 for the trip time of GFCI devices, which is calculated using Equation (1) [12].

$$T = \left(\frac{20}{I_F}\right)^{1.43} \quad (1)$$

where,

T=required trip time, s
I_F=fault current, mA

The required trip time for a 5mA ground fault is 7.26 seconds. As the fault size increases, the trip time decreases to ensure larger faults do not have sufficient time to cause injury or property damage.

For the AFCI detection design, the objective was to sense high frequency current signals representing arc fault produced noise. According to the National Electric Code (NEC), an AFCI is "a device intended to provide protection from the effects of arc faults by recognizing characteristics unique to arcing and by functioning to de-energize the circuit when an arc fault is detected" [13]. Arc fault detection requires complex algorithms to distinguish operational arcs from hazardous arcs. Therefore, Schneider Electric requested the arc fault detection component only needed to detect high frequency signals, which is a characteristic of both operational and hazardous arcs. The specified arcing current was a 100μA signal in a frequency range of 10 to 20MHz. The team decided to first conduct testing in a lower power setting using a 12VAC, 3.33A source for the AFCI prototype.

In order to create a competitive product, the team also intended to decrease the size and cost of the proposed design for the dual function breaker.

4. Design Approach

As explained in the project objectives, the team elected to perform testing at low power, 12VAC and 3.33A, as well as high power, 24VAC and 20A. Both prototypes were based on the same block diagram, which is shown in Figure 6.

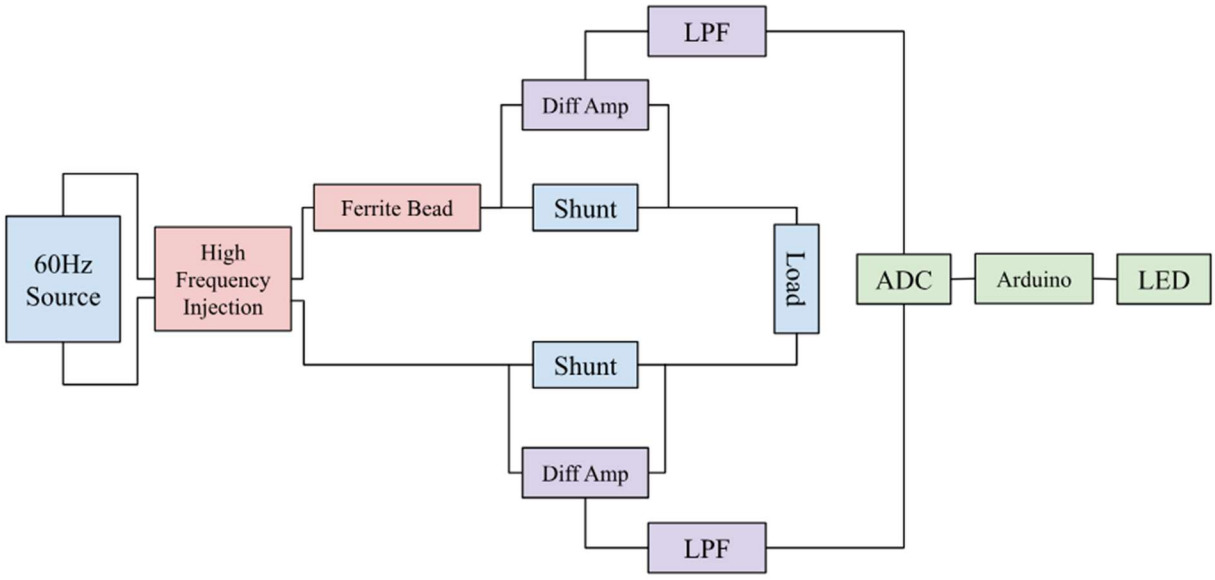

Figure 6. Proposed block diagram.

4.1 Source and Load

A 12VAC 3.33A AC/AC transformer was used for the low power test setup. Using a low power test setup reduced the risk of a harmful shock to team members or equipment during the trial-and-error phase of the project. To draw the intended current from the source, two 2Ω 50W resistors with 5% tolerance were used in series to create a 4Ω load resistance. The purpose of the load resistors is to complete the circuit with specified amperage. These resistors can be compared to running a series of incandescent light bulbs or a space heater and will not be included in the circuit breaker design. The low power source and load are pictured in Figure 7.

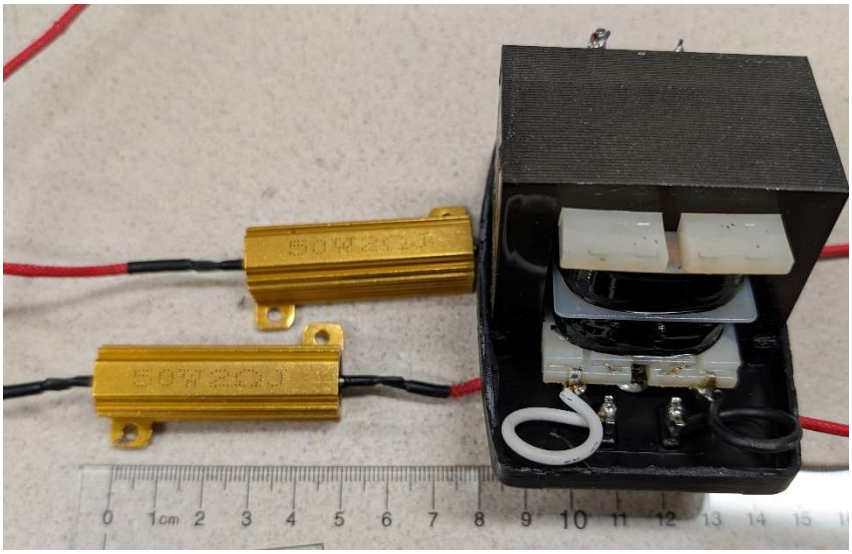

Figure 7. 12VAC transformer and 4Ω load for low power testing.

To implement the higher power 24VAC 20A test setup, two 120/24VAC 60Hz 10A transformers were wired in parallel, shown in Figure 8. As calculated using Ohm's Law, the 24VAC 20A setup required a 1.2Ω resistive load. Due to the high cost of a single 1.2Ω 480W rated resistor, three 0.4Ω 200W power resistors were used in series. The source and load for higher power testing are shown in Figure 9.

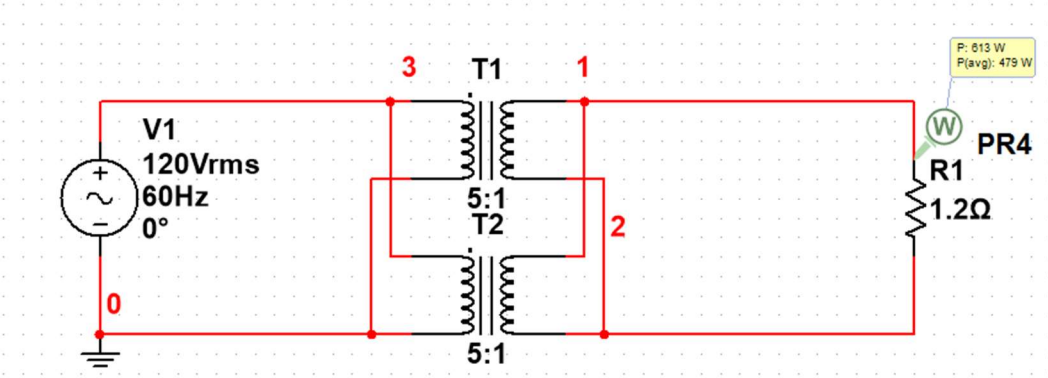

Figure 8. Parallel 240VA transformer setup.

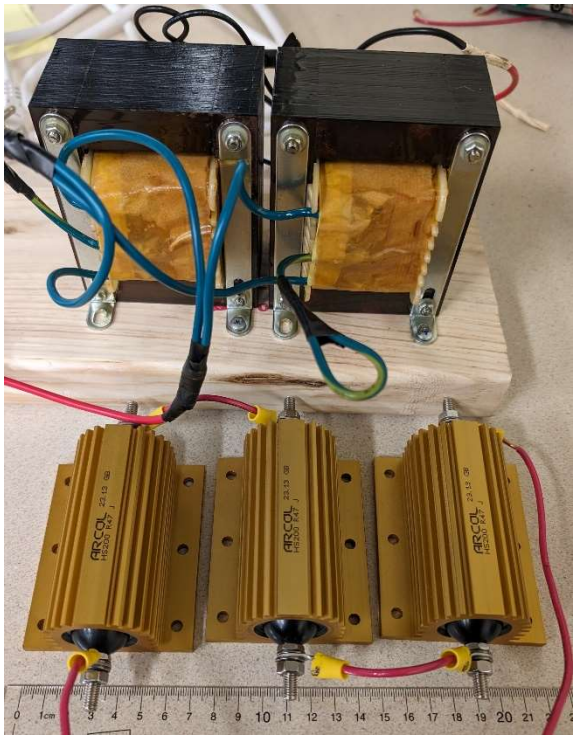

Figure 9. Two 24VAC transformers and 1.2Ω load resistors for high power testing.

4.2 Resistive Shunts

Shunt resistors are used to measure both AC and DC current by measuring the voltage drop across the resistor [14]. In selecting a material for the shunts, the team researched characteristics of several types of resistive materials, shown in Table 1. The most important characteristics to consider were temperature coefficient and noise. The temperature coefficient, α, indicates how sensitive the resistance is to temperature changes. A lower temperature coefficient means the resistance is less susceptible to change under different temperatures. Additionally, minimal noise, primarily thermal, is an important characteristic of the shunts because the fault current is only 0.025% of the load current, so any noise could cause a false trip. Based on these criteria, thick metal film or precision metal film would be the best choices, but the team selected the metal film material due to its lower cost.

Table 1. Characteristics of types of resistive materials [15].

Characteristic	Carbon Composition	Carbon Film	Thick Metal Film	Metal Film	Precision Metal Film
Temperature Range (°C)	-40 to +105	-55 to +155	-55 to +130	-55 to +125	-55 to +155
Maximum Temperature Coefficient (ppm/°C)	1200	1000	100	100	15
V_{max} (V)	500	500	250	350	200
Noise (μV/VDC)	4	4	0.1	0.5	0.1

The calculation for the shunt resistor value was based on the sponsor's specification to dissipate no more than 1W of power in the shunt. From a 20A source, the power dissipated in a shunt is calculated using Equation (2).

$$P = IR^2 \tag{2}$$

where,

P=power dissipated into resistor, W
I=current passing through resistor, A
R=resistance, Ω

In order to dissipate a maximum of 1W, the shunt resistors needed to be 2.5mΩ or less. The team selected 1.875mΩ metal film shunts with a temperature coefficient of 50ppm/°C. This is a standard temperature coefficient for resistors, however we found temperature changes will not have a major impact on the resistance. Equation (3) is used to calculate how resistance changes at varying temperatures.

$$R = R_{ref}[1 + \alpha(T - T_{ref})] \tag{3}$$

where,

R=conductor resistance at temperature T, Ω
R_{ref}=conductor resistance at reference temperature T_{ref}, usually 20°C, Ω
α=temperature coefficient of resistance for the conductor material, ppm/°C
T=conductor temperature, °C
T_{ref}=reference temperature that α is specified at for the conductor material, °C

Using 1.875mΩ shunt resistors with a temperature coefficient of 50ppm/°C, the behavior of a dual shunt resistor circuit with varying shunt temperatures was calculated as shown in Table 2. Further thermal simulations are included in Section 5.1 GFCI Simulations and Schematics.

Table 2. Shunt resistor values at varying temperatures.

Conductor Temperature (°C)	**R_{shunt} (mΩ)**
20	1.875
30	1.8759375
40	1.876875
50	1.8778125
60	1.87875
70	1.8796875
80	1.880625
90	1.8815625
100	1.8825
110	1.8834375
120	1.884375

4.3 Amplification and Filtering for Ground Fault Circuit Interrupter

To sense the voltage drop across the shunt resistors, difference amplifiers were implemented as seen in the block diagram in Figure 6. The difference amplifiers were selected due to their ability to handle high common-mode voltages. The common-mode voltage is the average voltage of the two input pins of an operational amplifier relative to the power supply pins [16]. In this project, the input pins were positioned on either side of the shunt resistors. One pin connects to the source voltage, while the other is connected to the source voltage reduced by the voltage drop across the shunt resistor. Given that the voltage drop across the shunt resistor is insignificant compared to the source voltage, the common-mode voltage approximates the value of the input signal. Specifically, for the low power test setup, the common-mode voltage is 12VAC, while for the higher power test setup, it is 24VAC.

When searching for a difference amplifier, the team identified the following specifications: low noise, adjustable gain, compatibility with a 5V single supply or ±15V dual supply range, and a minimum common-mode voltage of 24V. The INA145 programmable gain difference amplifier meets these specifications. It allows for differential gain ranging from 1V/V to 1000V/V, has a dual supply range of ±2.25 to ±18V, and provides a ±30V common-mode voltage for a ±15V

supply voltage, with low noise [17]. To achieve the required ±30V common-mode voltage range, the 5V supply from the Arduino was stepped up to ±15V using two IA0515S DC-DC converters to isolate the common ground for each shunt [18]. These converters receive a 5V input from the Arduino and deliver a ±15V output.

Figure 10 is the pinout schematic of the INA145. V_{IN}^{+} and V_{IN}^{-} connect to either side of the shunt sensing resistor. $V^{+}$and V^{-} connect to the +15V and -15V rails, respectively. Ref is connected to ground. R_{G1} and R_{G2} are the resistors used to set the programmable gain. The values were chosen based on the Equation (4), taken from the INA145 datasheet. For the low power test set up, R_{G1} and R_{G2} were chosen to be 100Ω and $4.3k\Omega$, respectively, to produce a voltage gain of 44.

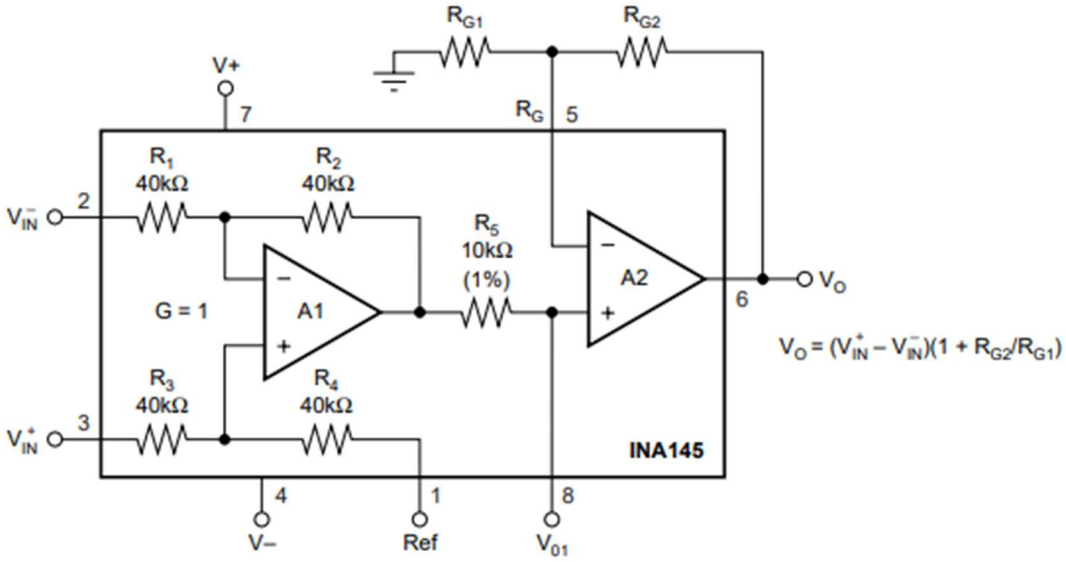

Figure 10. INA145 difference amplifier pinout [17].

$$V_O = (V_{IN}^{+} - V_{IN}^{-})\left(1 + \frac{R_{G2}}{R_{G1}}\right) \tag{4}$$

where,

Vo = output voltage, V
V_{IN}^{+} = input voltage before the shunt, V
V_{IN}^{-} = input voltage after the shunt, V
R_{G2} = $4.3k\Omega$, resistor between pins 5 and 6, Ω
R_{G1} = 100Ω, resistor between pin 5 and ground, Ω

The initial design phase focused on determining the necessary gain and minimizing noise in the circuitry. In the low power test setup, a detection sensitivity of 9.375μV was required for a 5mA fault. This value was derived using Ohm's Law based on a 1.875mΩ shunt resistance and the 5mA fault current. To interface with a microcontroller, the voltage signal needed to be amplified to at least 1mV, necessitating a minimum gain of 100. To achieve this, cascading amplifiers and a low-pass filter were employed to eliminate high-frequency noise. Low pass filters (LPF), as depicted in Figure 6, were positioned at the output of the difference amplifiers for this purpose.

First, a low-pass filter with a cutoff frequency of 80Hz and a gain of 4 was implemented for each line. Figure 11 shows the schematic of the active low-pass filter. For the construction, we used a standard LM741 operational amplifier and resistors and capacitors with a tolerance of 5%. Resistor matching mitigated the effect of tolerance variations. The calculation of resistor and capacitor values essential for attaining the specified cutoff frequency and amplification are based on Equations (5) and (6).

$$f_c = \frac{1}{2\pi R_3 C_1} \tag{5}$$

where,

$f_c = 80\text{Hz}$, cutoff frequency
$R_3 = 10k\Omega$, low pass filter resistor
$C_1 = 0.2\mu F$, low pass filter capacitor

$$A = \frac{R_2}{R_1} + 1 \tag{6}$$

where,

$A = 4$, gain
$R_2 = 3k\Omega$, amplification resistor between inverting terminal and output
$R_1 = 1k\Omega$, amplification resistor between inverting terminal and ground [19]

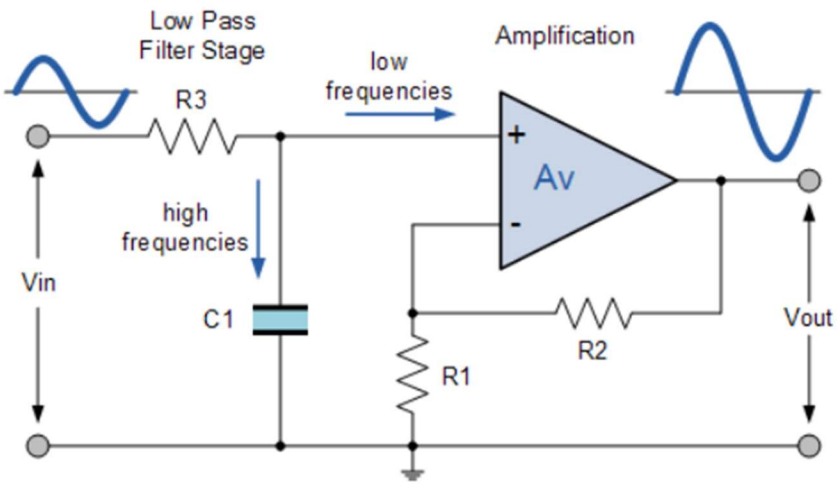

Figure 11. Active low-pass filter with amplification [20].

The construction of the low pass filters was followed by a characterization process, during which the team observed identical behavior in both filters. Each exhibited a gain of precisely 3.094 and demonstrated a similar frequency response, as illustrated in Figure 12. The frequency response was plotted using a function generator to step through frequencies at discrete points ranging from 20Hz to 1MHz. An oscilloscope was then used to measure the input and output voltages to calculate the gain. While a continuous frequency sweep would be preferable, the team did not have immediate access to a spectrum analyzer and therefore chose the step method as it would produce results accurate enough for analysis. After testing, it was found that the filters did not have a gain of 4 as designed due to the attenuation near the cutoff frequency at the 3dB point. This was rectified by adjusting the cutoff frequency to a value further from the system's operating frequency of 60Hz. A higher order low pass filter was not implemented because of their increased complexity. This increased complexity would introduce more sources of error and increase the circuit's overall cost and power consumption due to the larger number of components.

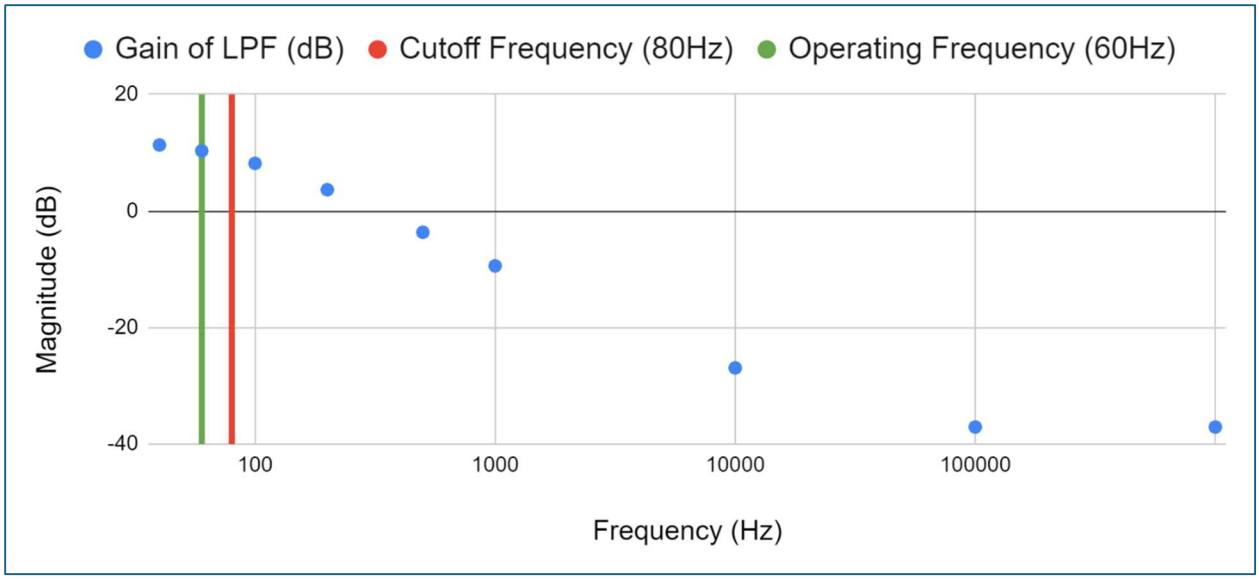

Figure 12. 80Hz low pass filter frequency response.

To eliminate the effect of attenuation near the operating frequency, the cutoff frequency was increased to about 1kHz. This choice ensures minimal attenuation at the 60Hz operating frequency while effectively blocking high frequency noise. Shifting the cutoff frequency by a significant margin allows noise between 60Hz and 1kHz to be amplified which is a larger range than the original 60Hz to 80Hz. To keep the amplified voltage signal within the input range of the ADC, the gain was kept at 3. Equations (3) and (4) were used to attain a cutoff frequency of 1061Hz and a gain of 3. The values of the low-pass filter were changed as follows: $R_1 = 1k\Omega$, $R_2 = 2k\Omega$, $R_3 = 1.6k\Omega$, and $C_1 = 0.1\mu F$. Once constructed, testing was conducted using a 110mV$_{pk\text{-}pk}$ 60Hz sine wave from the function generator into the difference amplifier utilizing the step method as described previously. Figure 13 displays the frequency response of the new amplifier, indicating no attenuation at the operating frequency, 60Hz. The roll-off of the low pass filter has a slope of approximately 15.5dB per decade. While this is a little low compared to the ideal case of 20dB per decade, it was deemed acceptable. To increase this roll-off the team would have had to implement a higher order low pass filter and as previously stated, the team did not want to add complexity due to power, noise, and cost concerns. Additionally, a 6-degree phase shift was observed between the input and the output signals of the low pass filters at 60Hz. However, this does not need to be considered because the ADC and Arduino sampling is configured in a way that does not rely on signal phase alignment. The phase was not plotted in Figure 13 due to its insignificance and limited access to a network analyzer.

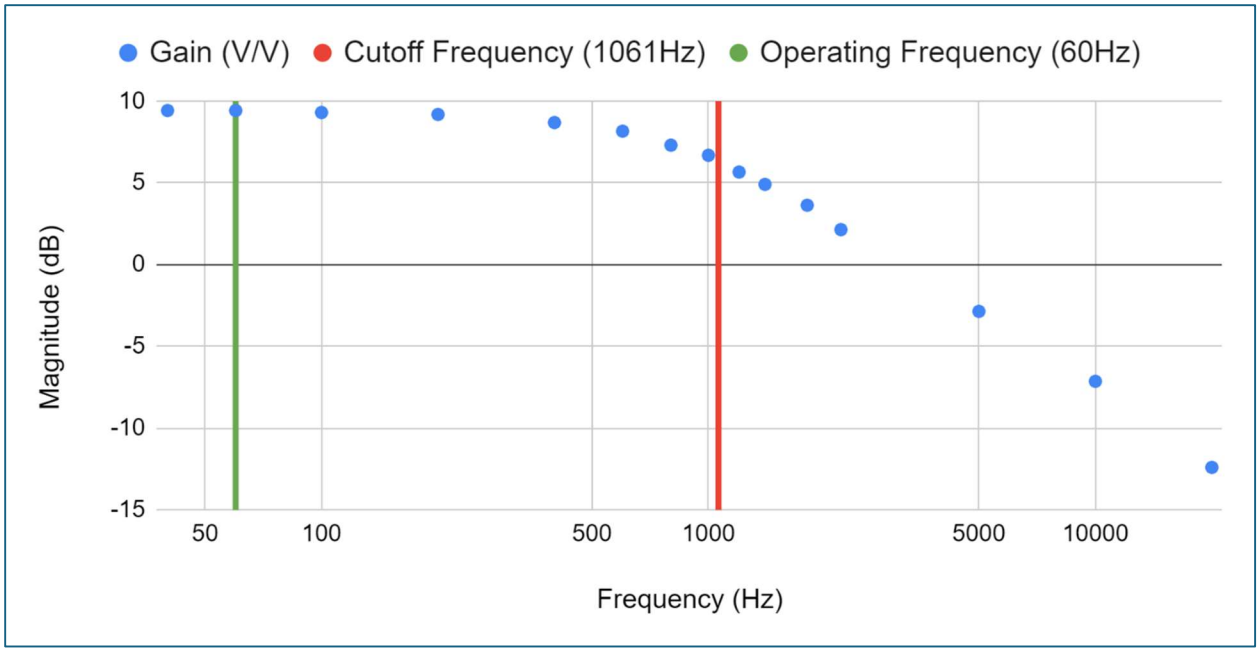

Figure 13. New low pass filter frequency sweep.

Once the difference amplifier and low-pass filters were configured, the pieces could be consolidated onto a breadboard as seen in Figure 14 and testing could be conducted to identify how the hardware was performing. Surface mount to through hole adapters were implemented, minimizing noise from the wire connections. Additionally, FR-4 solderable breadboards were utilized for sturdier connections and compactness.

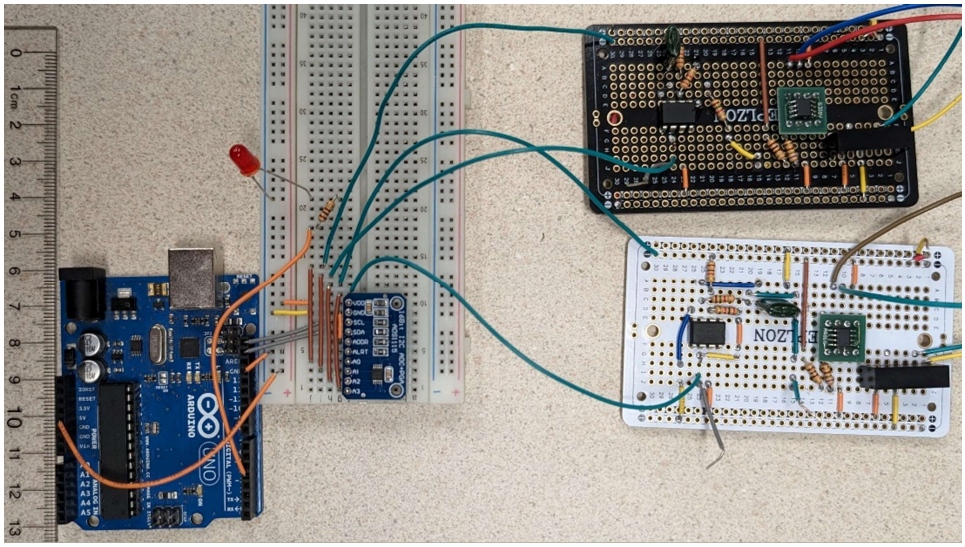

Figure 14. GFCI amplification, filtering, and signal processing circuit.

In this process, resistor matching was used to improve the similarity between the two amplifier circuits. Before resistor matching, the first difference amplifier had a gain of 45 and the second 38. After resistor matching, the first difference amplifier had a gain of 47 and the second 46. When the difference amplifier and low-pass filter stages were combined, both circuits had a gain of 116.

The final design for the low power circuitry included the use of the INA145 difference amplifier with a voltage gain of 46 in series with the 1kHz low-pass filter with a voltage gain of 3. This system effectively amplified the voltage drops across the shunts and filtered out extraneous high-frequency signals. The output signals of each side of the shunts were then routed to the ADC and Arduino for proof-of-concept analysis and tripping the breaker before any modifications were made for the higher power circuitry.

With this final design, the output signals of the amplification and filtering circuits could be read into the analog to digital converter (ADC). A problem during this process's early stages was that the ADC could not read the AC voltages on the two lines at the same time. This meant that the ADC would compare the two AC voltages at different parts of the waveforms so it would find the difference in magnitude caused by a phase variation rather than the difference in magnitude caused by a fault. One attempt to correct this problem was to use a rectifier. The idea was to convert the AC signal to a DC signal before inputting it into the ADC and Arduino. A basic half-wave rectifier was implemented as seen in Figure 15. While effective, the rectifier would be impractical in large scale production due to variability in diodes and capacitors. This is because the goal is to keep the circuitry on the live and neutral lines as identical as possible. Any variation, especially in the diodes, would add to the discrepancy between the lines which increases the likelihood of a false trip. Moreover, a more reliable method of sampling the signals was identified, which does not necessitate simultaneous sampling. Further details on this can be found in Section 4.4 Ground Fault Circuit Interrupter Signal Processing.

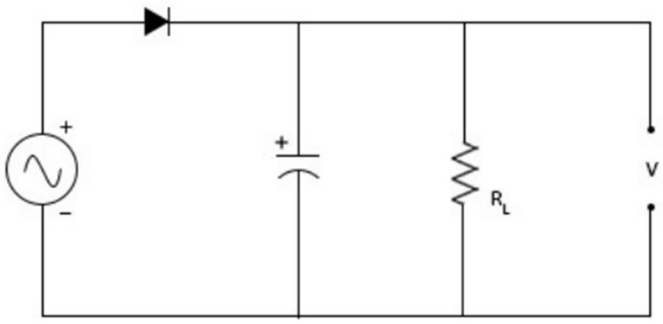

Figure 15. Half-wave rectifier [21].

4.4 Ground Fault Circuit Interrupter Signal Processing

To determine the difference between the voltages measured across each shunt, the team elected to use a microcontroller, specifically the Arduino Uno, to read the output signals from the low pass filters. The Arduino Uno has a built-in ADC, but it cannot be used to measure two voltage inputs without a common ground. A common ground could not be used between the shunts because it would eliminate their isolation and cause a short circuit.

Several external ADCs were considered and evaluated in Table 3. From the value analysis, the Aceirmc ADS1115 was selected for its low cost and analogous functionality to the Adafruit ADS1115.

Table 3. Value analysis of potential analog to digital converters.

	Analog to Digital Converter	Market	ADAFruit ADS1115		Aceirmc ADS1115		ARD-LTC2499	
Features		Weight	Value point	Total	Value point	Total	Value point	Total
1	Cost per unit	-4	14.95	-59.8	3.6	-14.4	55	-220
2	Resolution in Bits	5	16	80	16	80	24	120
3	Sample Time	3	860	2580	860	2580	15	45
4	Number of Differential Inputs	4	2	8	2	8	8	32
5	Compatibilty with Arduino	4	5	20	5	20	5	20
6	Ease of Programming	2	5	10	5	10	3	6
	Total			2638.2		2683.6		3

The default reading style of the ADS1115 is called continuous mode, which reads the input voltage values over 128ms and results in inconsistent readings of an AC signal. For this project, the reading style needed to be single shot mode, where the ADC measures the voltage at the positive or negative edge of a clock cycle, resulting in a new reading every 10µs.

To determine the value the circuit breaker should trip at, the code includes a calibration step at the beginning of each power cycle. The calibration procedure first takes the maximum ADC

reading over 1000 samples. To establish the trip value from this maximum value reading, the code adds a specified number of steps to the maximum. This value is saved as the "Trip Value." During prototyping for this project, the trip value was 3 ADC-steps above the maximum reading during the calibration stage.

The calibration process is essential for this prototype, as testing revealed fluctuations in the maximum step between tests. This variability is likely due to minor changes in the resistance of the load resistors as they heated up, which would cause a different voltage drop across the shunt resistors. This calibration also offers advantages for real world applications as it can accommodate variations in component tolerances and load values.

4.5 High Frequency Signal Injection

Ground isolation from transformers posed a challenge in creating an AFCI simulation with high frequency noise. Due to potential ground voltage differential, a function generator is unable to directly inject frequencies over the entire circuit. Therefore, Faraday's Law was utilized to induce a voltage over wire using windings.

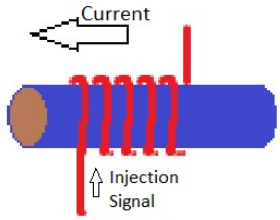

Figure 15. Drawing of wire windings.

$$\mathcal{E} = -N\frac{\Delta\Phi}{\Delta t} \qquad (7)$$

where,

Ɛ=induced electromotive force (emf) over the wire
N=number of turns of the wire windings
ΔΦ=change in magnetic flux
Δt=change in time

Using this equation with the given frequency parameters, 30 windings of 22AWG wire wrapped around the positive and negative 12AWG main wires induced 4mV over the ferrite bead and load when 400mV$_{pk\text{-}pk}$ was applied across the induction wire. The injection setup is shown in Figure 17.

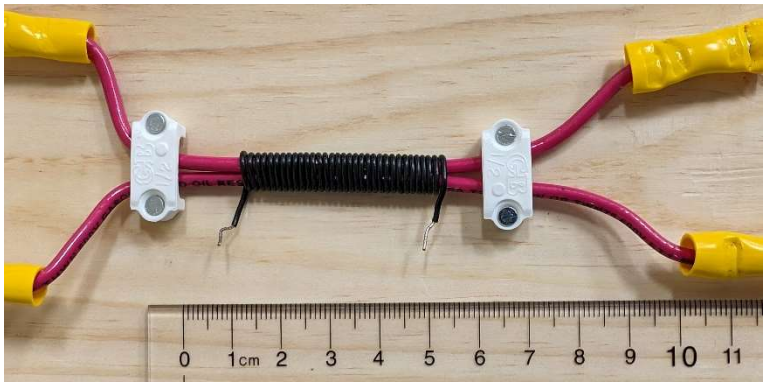

Figure 16. High frequency signal injection

As shown in Section 4.7, the Tai-Tech Ferrite Bead has an impedance of approximately 37Ω at 15MHz. Using Ohm's Law, we can further calculate the required voltage drop across our entire circuit when in series with the load of 1.41Ω, given a 100μA signal.

4.6 Arc Fault Circuit Interrupter Inductive Element Selection

To fulfill the arc fault sensing requirements as outlined by Schneider Electric, several conceptual designs were considered. Performance simulations were conducted to determine the efficacy and feasibility of each design, ultimately ascertaining which concept best fit the specifications.

Filtering and Amplification

This initial design looked to read the signal off the same shunt resistances as the GFCI detection circuit. The signal would be passed through a high pass filter to isolate the high frequency noise generated from the arc fault. This signal would also be amplified to a readable value.

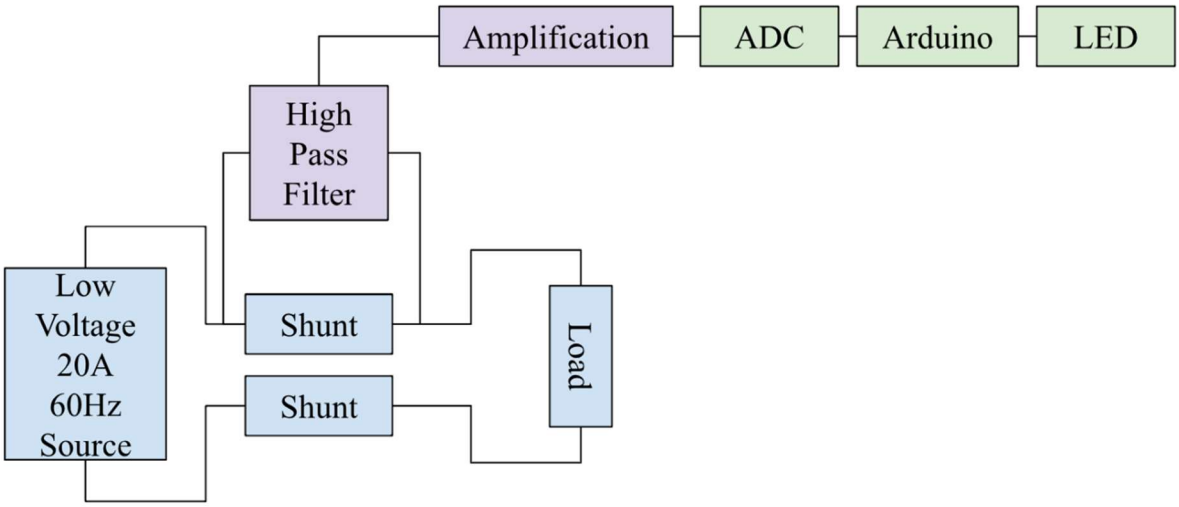

Figure 17. Block diagram of initial filtering and amplification design

This design minimized power loss along the power line but required many filtering and amplification components specialized to process high frequency signals. These components are comparatively expensive and introduce many potential variations in tolerances. Since small value resistors are required, as mentioned in Section 4.2 Resistive Shunts, a 100μA high frequency signal would create a voltage drop in the nanovolt range. Detecting this voltage would require excessive amplification and noise filtering that limit efficacy. Each stage would require a relatively large number of components which would undermine the core tenets of alternative AFCI detection — low cost and component simplicity.

Resonant Circuits

Additional designs that were investigated included resonant circuits. Both parallel and series resonant circuits were investigated and simulated to determine circuit response to varying frequencies. Containing only a resistor, capacitor, and inductor, resonant circuits are cheap to construct with few components.

In the series resonant circuit, the resonant frequency would be calculated around 60Hz, the main operating frequency. When noise in the high frequency range is injected, the reactance of the inductor would increase to create a voltage drop that would be detectable using the GFCI amplification components [22]. However, while this design has promise in ideal conditions, usage of real components have DC resistance that create constant impedance, even at resonant frequencies.

Parallel resonant circuits also appeared promising but also suffer from similar real-world limitations. With a high resonant frequency and while simulating an arc fault, the parallel combination of capacitor and inductor tends towards short circuit characteristics. This would bypass the resistor and create a change in voltage drop that would also be detectable by GFCI components [23]. Parallel resonant circuits suffer from similar drawbacks as series resonant circuits. Real components with internal resistance do not exemplify short circuit characteristics to the point that a voltage drop across the resistor would be sufficiently changed for detection.

Inline Inductors

The final proposed design for this project was to use an inline inductor to create increased impedance at higher frequencies. A breakdown representation of an inductor, such as a ferrite bead, includes a resistor, capacitor, and inductor in parallel, like the concept of a parallel resonant circuit. This inductor would be placed inline before the GFCI sensing shunt resistor. Power loss would be minimal as DC resistance of an inductor is relatively low. With high frequency input, the impedance increases from low impedance at the 60Hz operational frequency, to high impedance at the requested detectable 10-20MHz. This voltage drop would be detectable with a signal processor, tripping the breaker.

Inductor Characteristics

As an inline inductor was determined to be the best fit to satisfy sponsor requirements, several inductors were researched and tested. The table below shows the three chosen inductors [27, 40, 41].

Table 4. Tested inductive resistors

Inductor	DC Resistance	Impedance	Rated Amperage	Cost
Tai-Tech Ferrite Bead	1mOhm	65 Ω @25MHz	30A	$0.23
Wurth Ferrite Bead	0.9mOhm	65 Ω @25MHz	18A	$0.68
Vishay Inductor	2.34mOhm	157 Ω @25MHz	24A	$1.23

These inductors were chosen as they have low DC resistance that will minimize power loss and potential thermal drift. Being in line with the load also requires relatively high rated amperage,

20.0 A_{RMS}, which limits the options for inductors. In addition, these inductors have high impedance near the specified frequency band that allows the small current to create a voltage drop.

4.7 Inductor Testing and Filter Design for Arc Fault Circuit Interrupter

After reducing the number of inductors suitable for this project, the team created a simple voltage divider to calculate the impedances at different frequency levels. After creating the divider with a 50Ω resistor to impedance match the oscilloscope, the inductor's voltage drop at different frequencies was found to calculate their impedances. The table below shows the impedances of each inductor from 10kHz to 20MHz.

Table 5. Impedance results for inductors.

Frequency (MHz)	**0.001**	**0.01**	**0.1**	**0.75**	**1**	**5**	**7.5**	**10**	**15**	**20**
Wurth Impedance (Ω)	0.62	0.83	0.83	6.41	10.57	45.47	41.28	38.06	31.70	28.12
Vishay Impedance (Ω)	0.26	0.26	2.96	3.07	3.13	7.33	8.76	10.20	14.85	14.35
Tai-Tech Impedance (Ω)	0.62	0.83	0.83	3.48	5.65	33.91	35.05	32.79	37.44	27.15

Plotting the impedance values on the same graph in Figure 18, we can see which inductor is best for the project requirements of detecting a signal in the 10-20MHz range. The Tai-Tech ferrite bead best met this objective, as it has negligible impedance at 60Hz and a higher impedance at 15MHz.

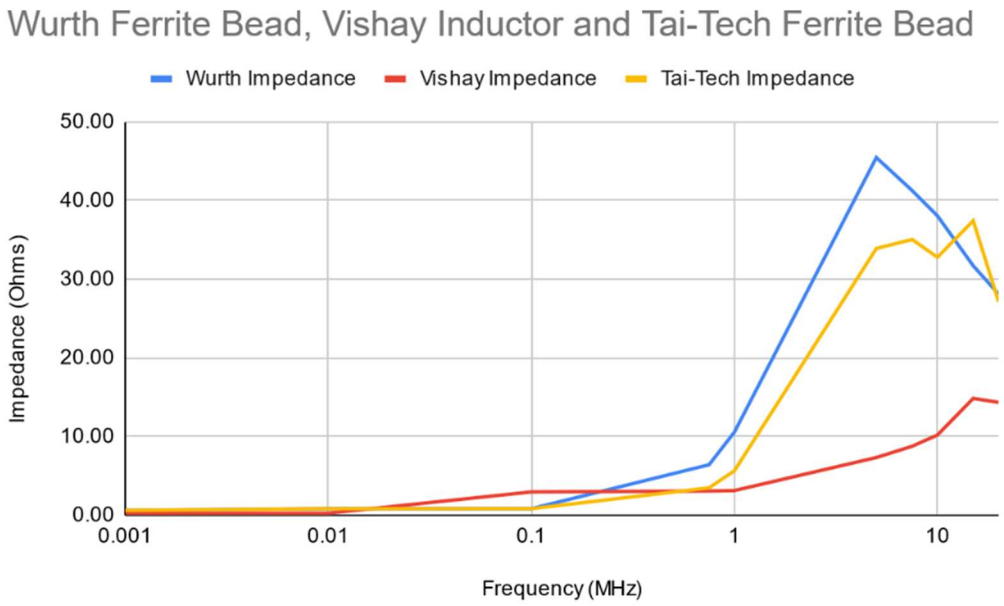

Figure 18. Ferrite bead impedance testing results.

Following this testing, Schneider Electric provided the team with more accurate data using a NANO Vector Network Analyzer [39]. The sponsor was able to determine the impedance of the ferrite bead to be closer to 41Ω. Using Ohm's Law, the voltage drop from a 100µA signal was calculated as 4.1mV.

The voltage drop over the ferrite bead provides an acceptable amplitude for detection. However, the measured output voltage was still noisy and could cause false trips with signal impulses. In order to attenuate noise over the ferrite bead at high frequency time scales, a low pass filter was considered for implementation. Using an integrated circuit (IC) filter would provide the most effective attenuation while maximizing pass-band signal amplitude. However, IC filters satisfying design requirements are cost prohibitive, exceeding the cost of the low frequency filters utilized in current circuit breaker designs.

Usage of oscilloscope bandwidth filtering beyond 20MHz effectively attenuated the signal noise. For this reason, an LC low pass filter design using a 510nH inductor and 47pF capacitor with a resonant frequency of 31.75MHz was assembled. Since the amplitude of the ferrite bead's voltage drop is small, minimizing -3dB roll-off before the cutoff frequency is vital. Therefore, a resonant frequency above the required 10 to 20MHz sensing frequency was chosen.

While amplification can be utilized to offset the negative effects of a filter, high frequency specific components would be required. This would increase cost and potentially create amplifier noise or degradation of the signal. This was not necessary with our given sponsor requirements. With the filter attached, 1mV of the 4mV signal was attenuated, but remained relatively clean without any oscilloscope filtering.

4.8 Arc Fault Circuit Interrupter Signal Processing

Detecting an occurring arc fault requires the microcontroller to recognize a fault indicating signal. To do this, a similar detection method to GFCI would be used. However, instead of comparing the results from two separate ADC differentials as in the GFCI design, the value of only one of the ADC differentials would be considered. To determine the standard voltage drop across the ferrite bead, an autocalibration would have to be run under no fault conditions. Then, similarly to GFCI, a trip value would be set by adding a specified step value to the maximum reading during the calibration. Other than the number of ADC channels used, this detection method for AFCI is similar to GFCI detection.

4.9 Higher Power Modifications

With the low power proof-of-concept functioning, the team could move to combining GFCI and AFCI circuitry and the higher power testing to meet the requirements given by Schneider Electric. First the test set up was changed from the 12VAC 3.33A transformer to the 24V 20A transformer.

For the GFCI circuit to operate with the higher power setup, the nominal gain of the differential amplifiers had to be reduced from 44 to 8.5 to ensure the output would not exceed the $\pm 15V$ rails. To do this, the resistor R_{G2}, as seen in Figure 10, was reduced from a value of $4.3k\Omega$ to 750Ω. The goal was to amplify the voltage drop across the shunt resistors to about 1V before going into the low pass filter. The low pass filter and microcontroller were not modified from the low power circuitry.

Adjusting the AFCI circuit for higher power operation was minimal. The ferrite bead is rated properly for higher power amperage, the current coil injector is independent of the power source, and reading over the ferrite bead is not significantly affected by a change in load voltage

or current. Therefore, there were no major changes to the AFCI setup when moving to the final testing setup.

Figure 19 shows an annotated photo of the final test setup. When the GFCI amplification and filtering circuits were connected to the shunts, the output signal was $3.2V_{pk\text{-}pk}$. Ferrite bead readings were $4mV_{pk\text{-}pk}$ at 15MHz. Both signals provided an acceptable voltage level for the microcontroller to process.

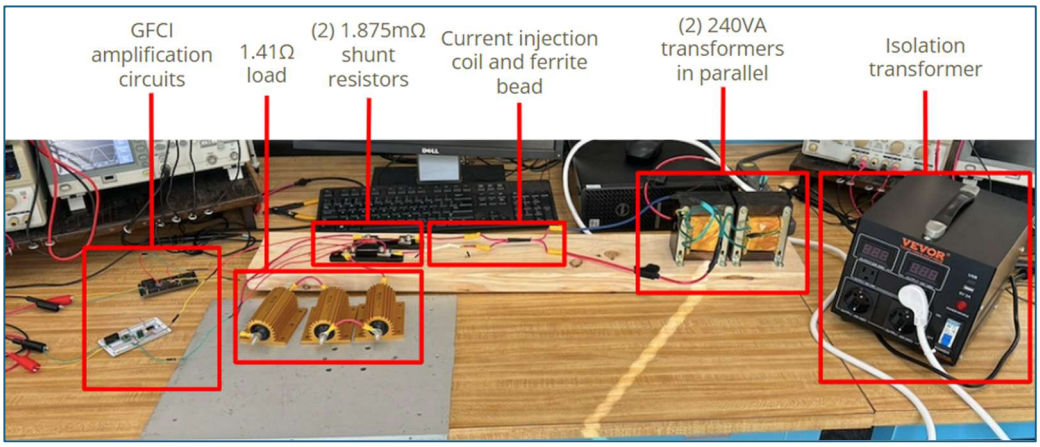

Figure 19. Final test setup for combined GFCI and AFCI.

5. Detailed Circuit Description and Simulations

5.1 Ground Fault Circuit Interrupter Schematic and Simulations

Throughout the GFCI design process, each circuit iteration was modeled and simulated in NI MultiSim to test its predicted behavior and bring attention to any design flaws before the physical circuit was constructed. The detailed GFCI schematic is shown in Figure 20. The GFCI circuitry was also modeled in LTspice for compatibility with Schneider Electric's tools. This simulation model can be found in Appendix C.

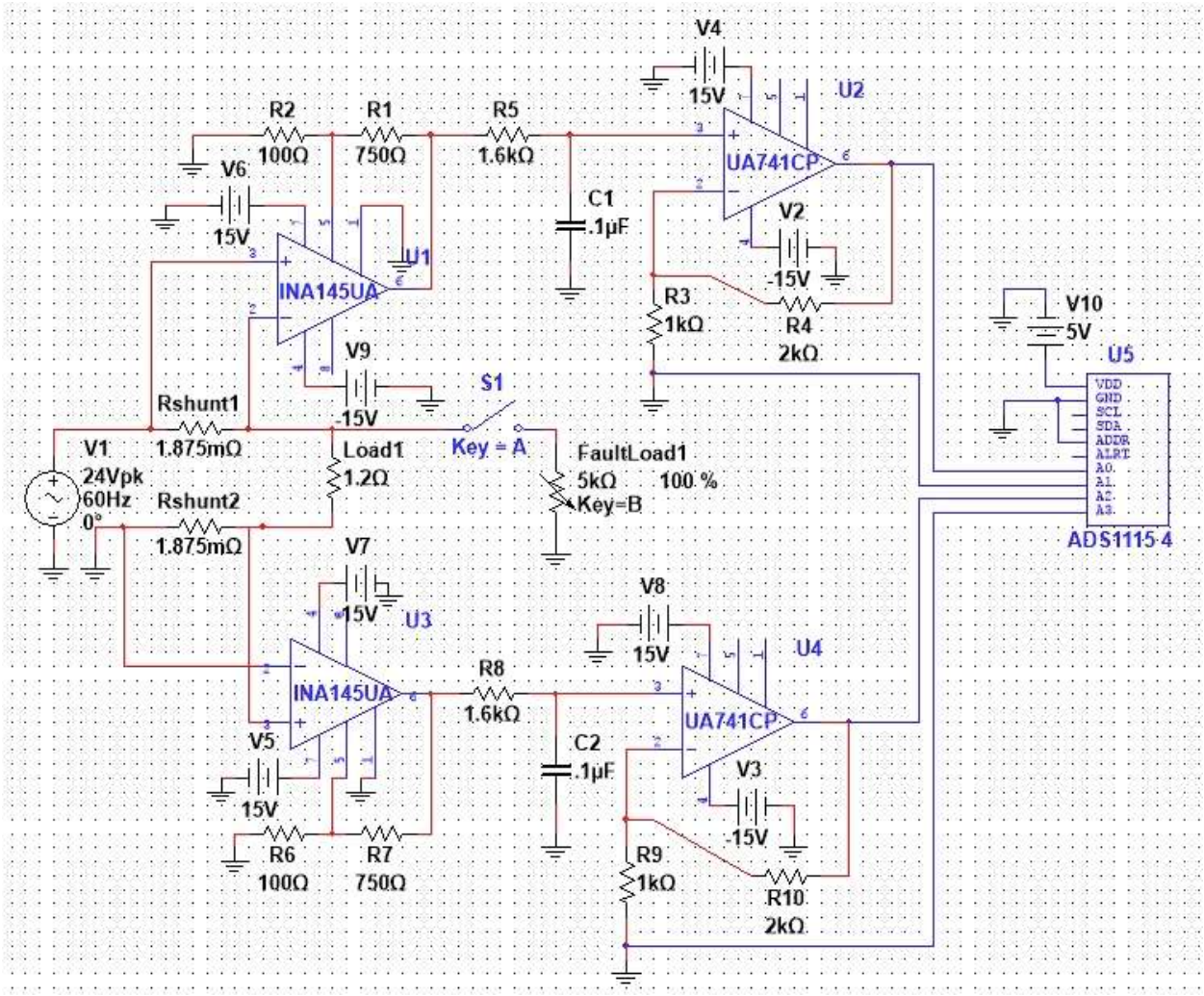

Figure 20. GFCI schematic for 24V/20A setup.

Each design iteration was simulated under no fault and fault conditions. Switch S1, shown in Figure 20, was open under normal conditions and closed to simulate a ground fault. A 5kΩ fault load corresponds to a 5mA ground fault at $24V_{RMS}$. The purpose of these simulations was to measure the differential voltage between ADC inputs A0 and A2 to ensure a ground fault would be detectable. The graph in Figure 21 below shows a simulation of a ground fault occurring. As measured by the cursors, the differential voltage under normal conditions was 30.3663mV and the differential voltage under fault conditions was 30.7352 mV, giving an expected voltage change of 369µV when a 5mA ground fault occurs. The minimum measurable step of the ADS1115 is 125µV, so this voltage change is significant enough to be detected by the ADC.

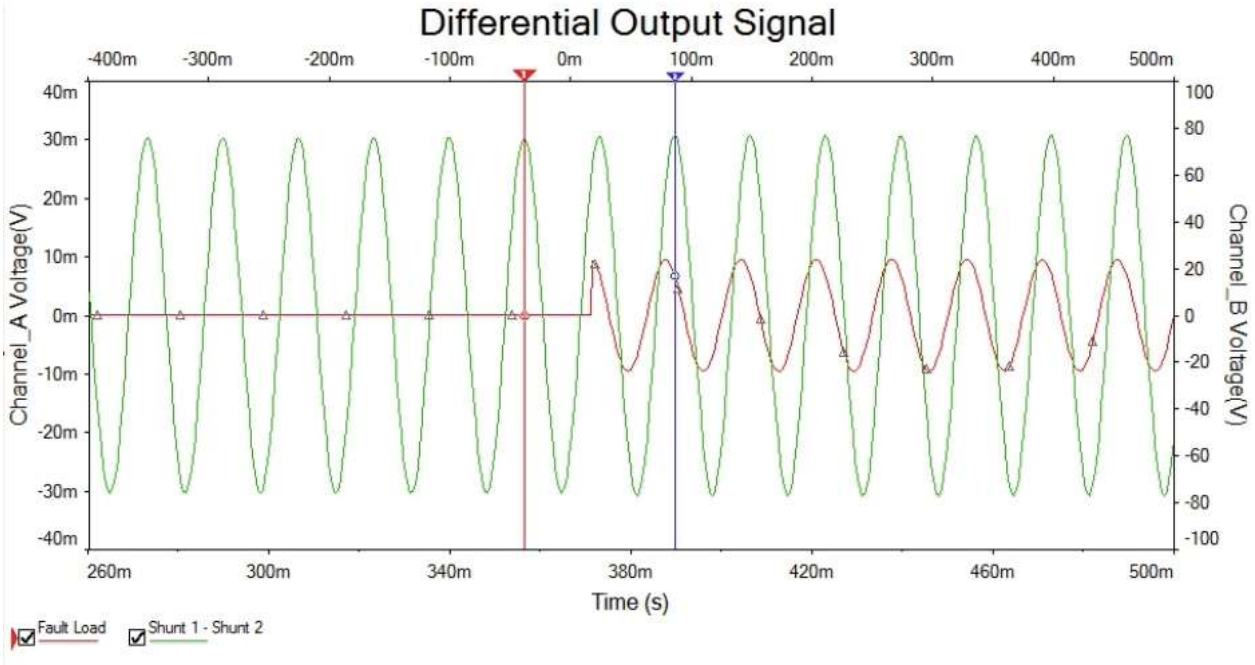

Figure 21. Differential voltage signal before and after ground fault.

Thermal behavior was taken into special consideration since any difference in temperature between the shunt resistors would cause them to have unequal resistances and, therefore, unequal voltage drops would be measured across them. To test the limits of a detectable fault with the shunts at different temperatures, a temperature sweep simulation was performed from 0°C to 300°C. This 300°C temperature swing was to test the worst-case scenario to ensure there would be no false trip in a real-world scenario. MultiSim uses a quadratic temperature model to provide more accurate impedance representations of resistors. One shunt was kept at a constant 25°C and the temperature of the other shunt was increased. As shown in Figure 22, there is no overlap between normal and fault conditions until the temperature difference between the shunts is 254.3°C. To avoid this issue that would cause a false trip, the shunts need to be in close thermal proximity in the circuit to keep them at a similar temperature.

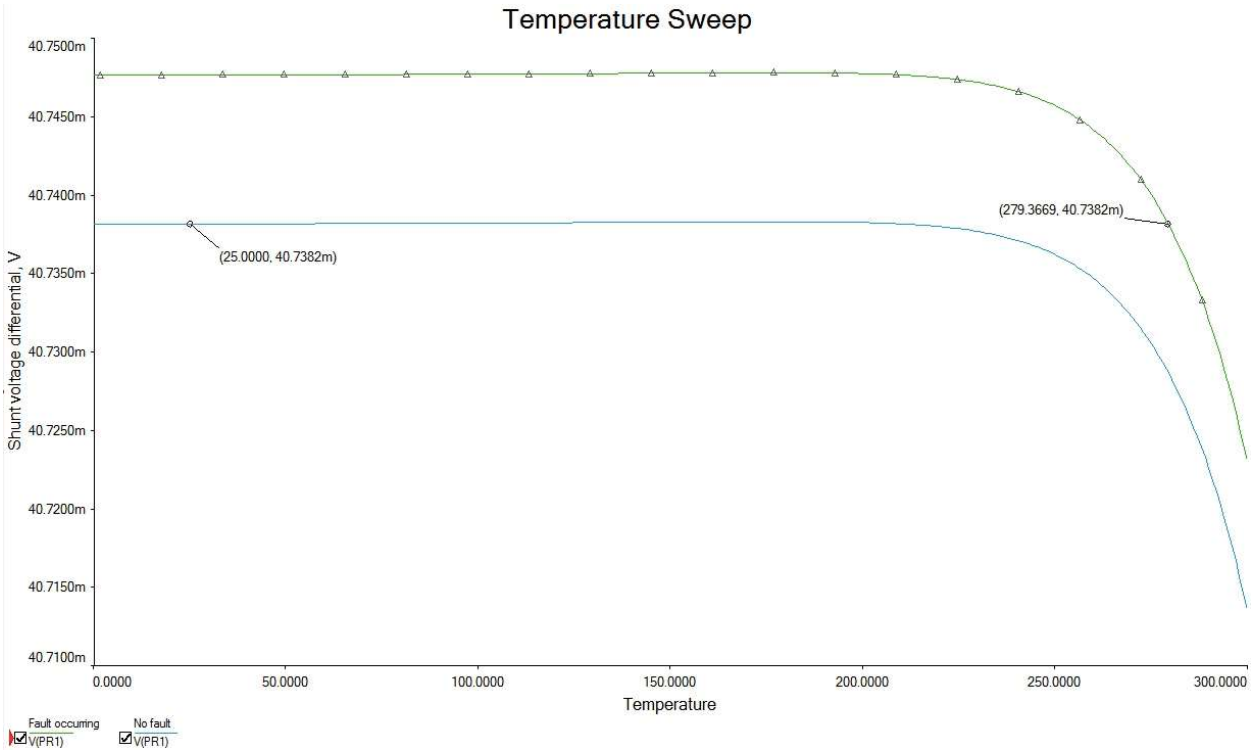

Figure 22. Temperature sweep of GFCI circuit before and after 5 mA ground fault.

The impacts of resistor tolerances and noise were also studied during simulations since variation in the differential output signal due to mismatched resistor values or noise could cause a false trip. In initial design stages, simulations showed that using a 150V/V gain differential amplifier made from the LM741 op-amp resulted in too much noise to detect a trip, even in a low power simulation. The output signal of this design is shown in Figure 23. Although the signal to noise ratio (SNR) was measured as 49.44dB, the more important factor is the change in signal when a fault occurs compared to the noise. In this simulation, the range of the noise was 20mV and the signal average only changed by 1.5mV when a fault was simulated.

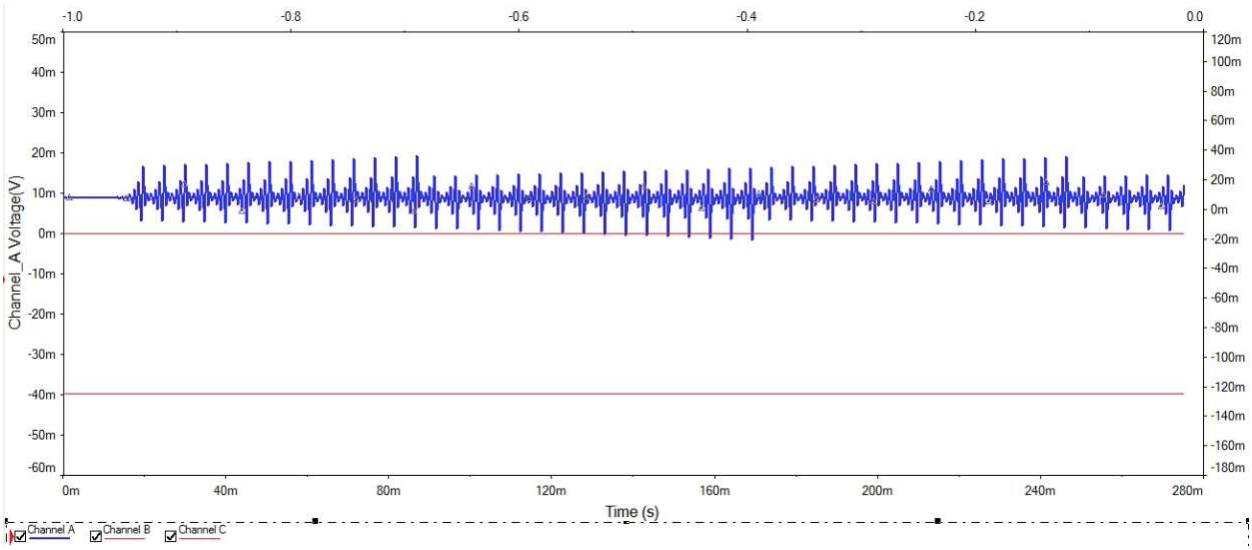

Figure 23. Noisy output signal from differential amplifier with gain of 150.

By using prepackaged differential amplifiers, transitioning to cascading amplifiers with lower gains, and adding a low-pass filter, the noise was limited to ensure faults could be accurately detected. The frequency sweep simulation results in Figure 24 show how the low-pass filter limits signals over 1000Hz, contributing to decreased noise in the circuit.

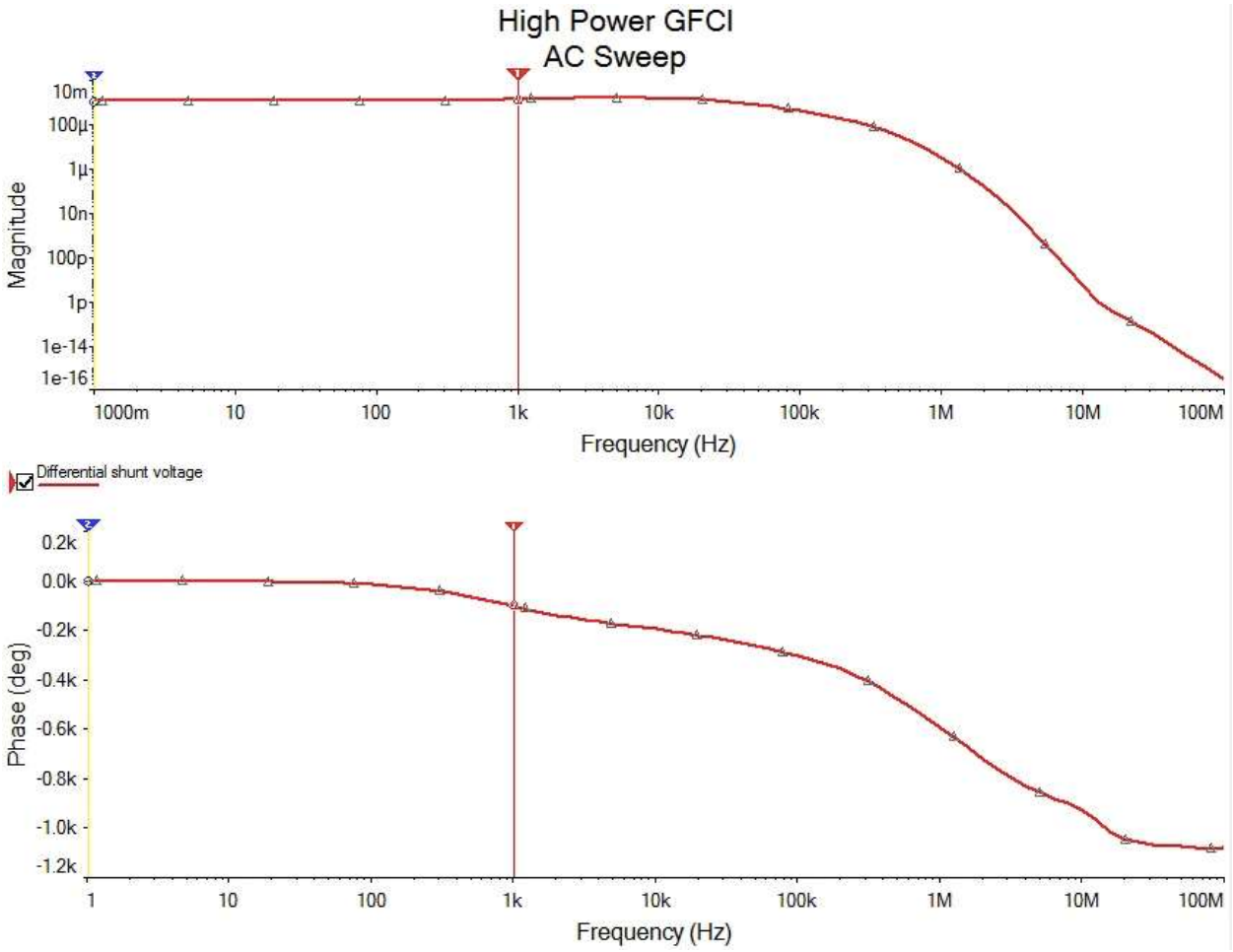

Figure 24. Frequency sweep for GFCI circuit.

A simulation was performed to observe the impact of resistor tolerances and determine the maximum resistor tolerances that would still allow a fault to be detected. Although individual resistors were matched in the amplifiers for the physical prototype, this is not realistic for large scale manufacturing. For resistor tolerances decreasing from 5% to 0% (ideal), the differential output voltage was found before and after a fault occurred. As reported in Table 6, the measured differential output voltages increased significantly as resistor tolerance increased, but the impact of the fault had minimal variation. Since resistor tolerances do not change as a result of a fault, only the impact of the fault is needed for detection. This simulation focuses only on worst case tolerances, not on worst case thermal drift, which would also cause fluctuations in the differential output voltage. The team opted to address thermal concerns through resistor selection and signal processing, as discussed in Sections 4.2 and 4.4.

Table 6. Resistor tolerance simulation results.

Resistor Tolerances (%)	V_{shunt1}-V_{shunt2} (mV)		Impact of Fault (mV)
	No Fault	Fault Occurring	
5	282.82364	283.23162	0.40798
1	87.30084	87.66074	0.35990
0.5	62.02841	62.38277	0.35436
0 (ideal)	28.41359	28.76079	0.34720

As mentioned in Section 4.4, Ground Fault Circuit Interrupter Signal Processing, autocalibration was incorporated into code to determine the differential output voltage under no fault conditions. This solution eliminates the possibility of false trips caused by noise or unmatched resistor values since it is only comparing the differential output before and after a fault occurs rather than comparing it to a set value. This feature reduces dependency on high precision resistors however because a GFCI needs to detect a fault immediately on power up, there would still need to be a combination of factory calibration and low-drift components.

5.2 Arc Fault Circuit Interrupter Schematic and Simulations

After finalizing the AFCI sensing component as an inline ferrite bead, LTspice was used to simulate an arc fault through the injection of a secondary voltage source. Figure 26 shows the circuit consisting of the source voltage and injection voltage in series, the ferrite bead, the shunt resistors, and the load resistors. Since LTspice does not have a proper component model for the ferrite bead, the bead is modelled as a resistor in series with a shunt configuration of capacitor, inductor, and resistor.

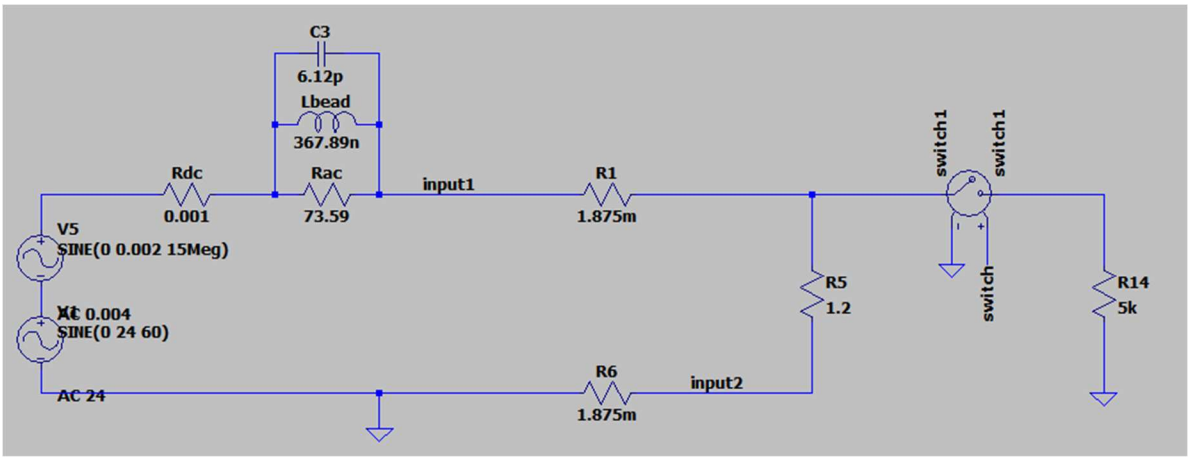

Figure 25. LTspice AFCI circuit schematic for 24V/20A setup.

The properties of the ferrite bead were calculated through information from its datasheet and a vector network analyzer. Since data from the VNA is more accurate, the ferrite bead component values in LTspice are taken from its measurements rather than our own calculations. The VNA was able to process the properties of the ferrite bead at different frequencies. The values used in the simulations are values taken from the properties of the ferrite bead at around 15MHz. The main voltage source is the 24VAC/20A 60Hz signal. The second voltage source is an injection of higher frequency voltage of 0.0133V at 15MHz. The amplitude of the injected voltage was calculated using Ohm's Law for the required 100µA signal across the 41Ω resistive element of the ferrite bead. In Figure 27, the voltage drop across the ferrite bead is plotted. In LTspice, the voltage drop is measured across R_{dc} and the parallel combination of C3, L_{bead}, and R_{ac}. As observed in the plotted simulation results, the voltage drop across the ferrite bead is around 4mV which gives a 100uA signal. The transient shows that the signal takes less than 1µs to stabilize and reach the $4mV_{pk\text{-}pk}$.

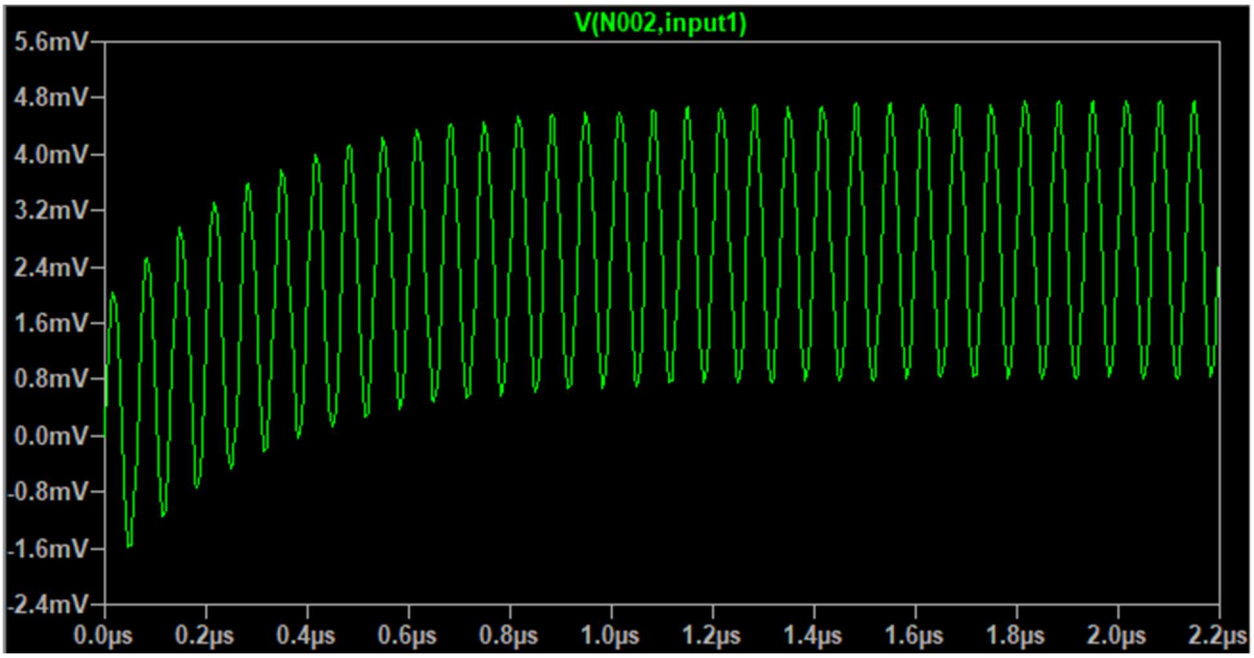

Figure 26. LTspice voltage across ferrite bead.

5.3 Combined Dual Function Breaker Schematic and Simulations

The combined ground fault and arc fault interrupter design was modeled in LTspice as seen in Figure 27. This simulation allowed for analysis of the integrated AFCI and GFCI circuit's performance, assessing potential interactions or interferences between them.

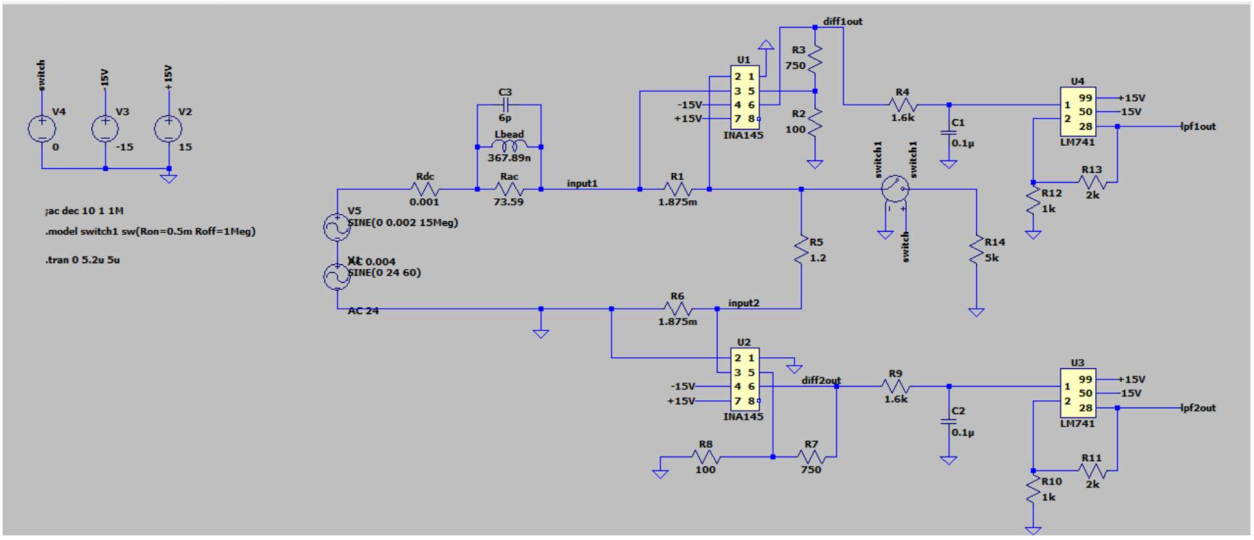

Figure 27. Combined AFCI and GFCI schematic in LTspice.

For verification of GFCI circuitry, the voltages across the shunts were measured. Both shunts showed a 37mV voltage drop across them as seen in Figure 28 and Figure 29. This voltage aligns with the results obtained from the GFCI LTspice model detailed in Appendix C. However, it deviates by 23% from the results of the GFCI NI MultiSim model. This discrepancy is likely due to variations in the software's algorithms for solving circuit equations, the specific component models used, and differences in the default simulation environments and the effects this has on the specific software's component models.

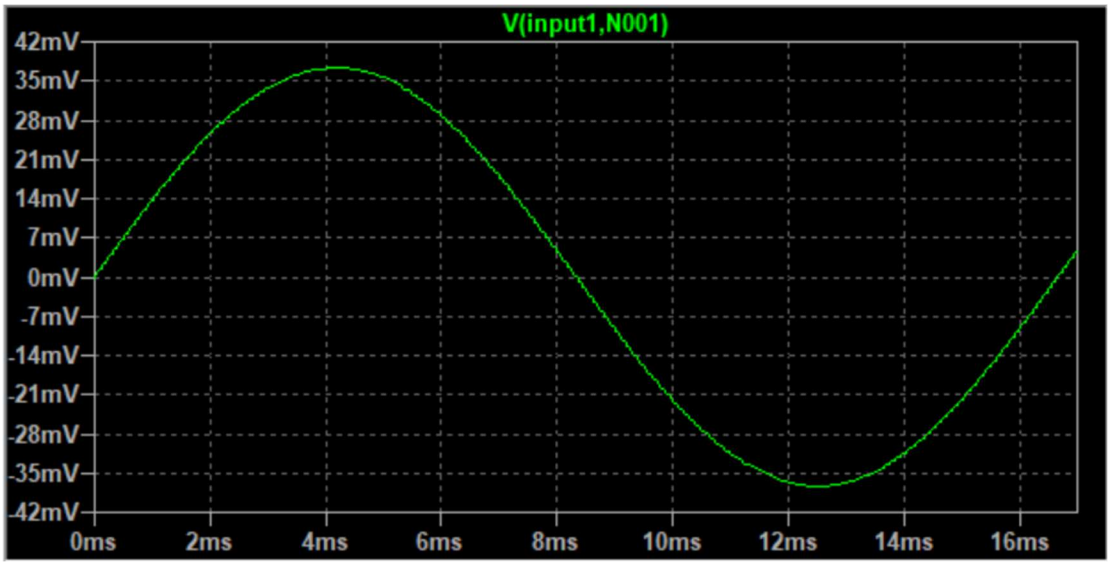

Figure 28. Shunt 1 voltage drop.

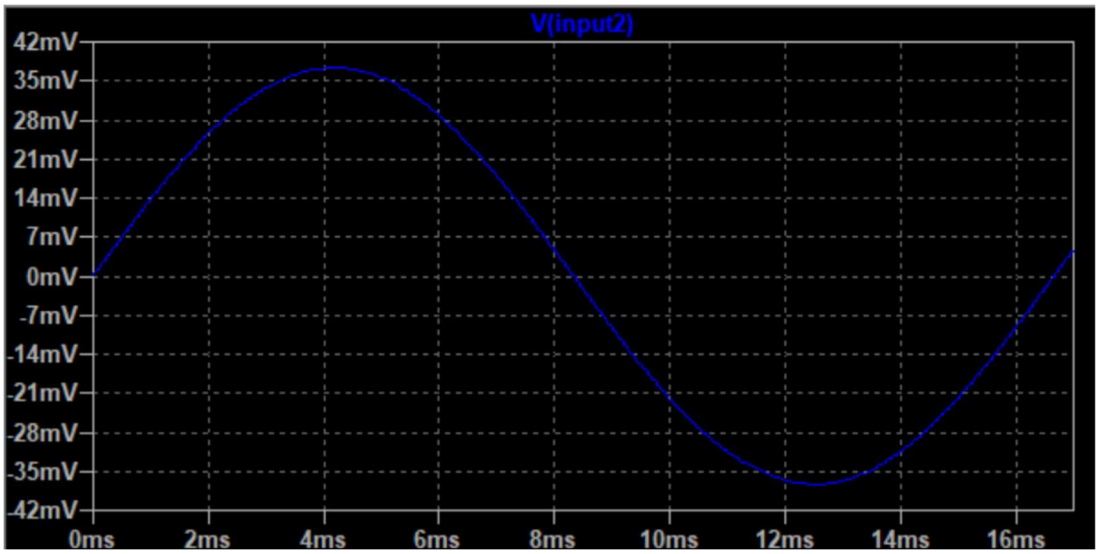

Figure 29. Shunt 2 voltage drop.

For verification of AFCI circuity, the voltage drop across the ferrite bead should be 4mV. There should also only be a 100µA signal across the ferrite bead, as it should be cutting out the 60Hz source signal. Figure 30 shows that the simulation results match the expected 4mV drop across the ferrite bead.

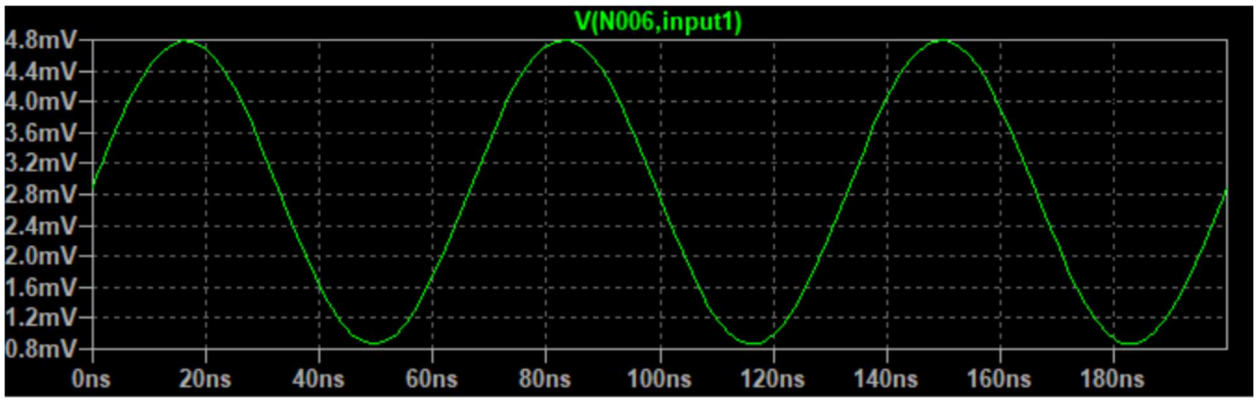

Figure 30. Voltage across ferrite bead.

From this model, the team was able to prove that the two circuits, GFCI and AFCI, will work simultaneously. The expected voltage drop was measured across both shunts for the GFCI requirements and a 100µA signal created a 4mV drop across the ferrite bead for the AFCI requirements.

6. Results

6.1 Higher Power Testing Results

After the high-power testing setup was assembled according to the schematic in Figure 27, testing was performed separately for GFCI and AFCI functionality. The increase in power from the 12V 3.33A setup caused the shunt and load resistors to get significantly hotter than the low power testing, consequently limiting testing duration to prevent overheating. This setup could be run for approximately 3 minutes with a fan for active cooling of the resistors. It took roughly 5 to 7 minutes for the power resistors to cool down between tests.

To test the response of the GFCI device to a ground fault, faults of decreasing current values were simulated by using resistors to bypass one of the shunts. The resistance values used to test for ground faults ranged from 250Ω to 5.1kΩ. The 250Ω fault resistor corresponded to a 102mA ground fault and the 5.1kΩ resistor corresponded to a 5mA ground fault. A 10kΩ resistor was also used to create a 2.5mA ground fault to test whether the system would trip for fault currents below 4mA.

Figure 32 shows the output signal of the GFCI amplification and filtering circuits once attached to the shunt. In order to test the functionality of the circuits without the microcontroller, the peak-to-peak voltage was measured with an oscilloscope before and after a fault occurred. A 250Ω fault resistor was used for a 96mA ground fault simulation to ensure a measurable difference could be detected by the scope. Before the fault occurred, the peak-to-peak voltage was measured as $3.26V_{pk\text{-}pk}$. The 102mA fault simulation increased the peak-to-peak voltage by 40mV, resulting in a $3.30V_{pk\text{-}pk}$ measurement. The output change due to the ground fault was reflected instantaneously on the oscilloscope.

a. b.

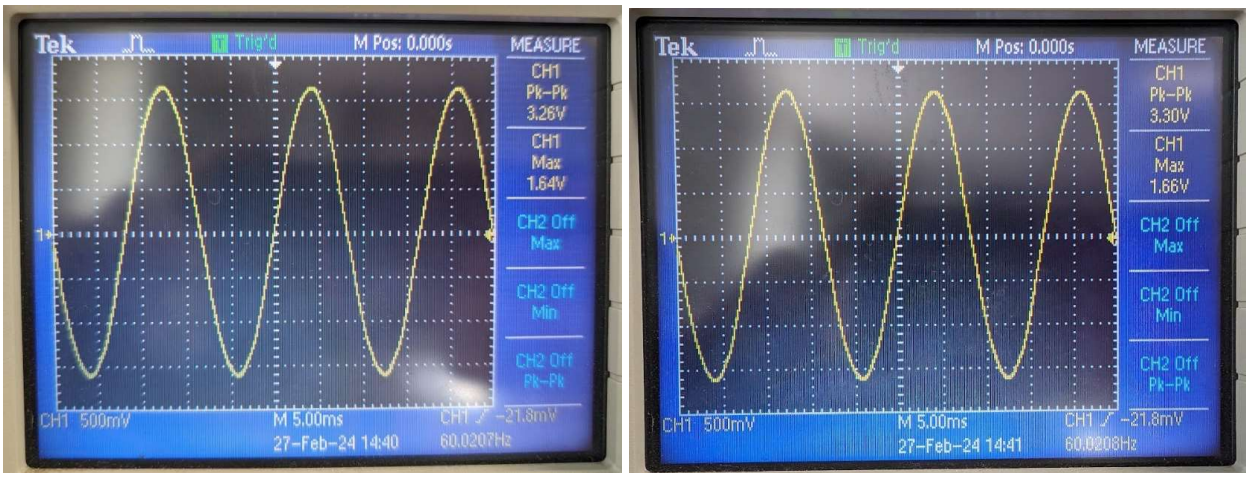

Figure 31. GFCI output signal (a) normal conditions, (b) 102mA ground fault simulated.

Based on the successful results measured with the oscilloscope, the full GFCI setup was tested using the ADC and Arduino as described in Section 4.4 Ground Fault Circuit Interrupter Signal Processing. For each of the 500Ω, 1kΩ, 2kΩ, and 5.1kΩ fault resistors, a minimum of four simulation trials were performed. When the fault was initiated, the trip time was measured. If the microcontroller did not detect the trip within 90 seconds, the trial was ruled inconclusive to prevent overheating of the load resistors. The data collected from the successful trials of each fault resistor is displayed in Table 7. Furthermore, it was found that for the 2.5mA fault current using the 10kΩ resistor, the system did not trip.

Table 7. Trip time of GFCI device for different fault current values.

Fault Resistor Value (Ω)	500Ω	1kΩ	2kΩ	5.1kΩ
Fault Current (mA)	51.2	25.6	12.8	5.02
Trial 1 Trip Time (s)	26.28	4.89	32.03	24.65
Trial 2 Trip Time (s)	8.32	21.22	45.00	42.49
Trial 3 Trip Time (s)	38.65	45.42	13.10	6.41
Trial 4 Trip Time (s)	10.24	14.70	41.61	37.01
Average Trip Time (s)	**21.5575**	**24.445**	**38.515**	**27.64**

To read off the arc fault monitoring components, the signal was applied across the signal injector, resulting in the desired 100µA 10-20MHz arc fault representation. From this injection, a

$4mV_{pk\text{-}pk}$ waveform was read across the ferrite bead using a handheld oscilloscope. When injecting a signal without any connection to the 60Hz power source, there was a clean 4mV signal across the ferrite bead. When the 60Hz source was connected, the signal was distorted with noises from other frequencies. To rectify this, the low pass filter with a resonant frequency of 31.75MHz was implemented. By attenuating signal components greater than desired frequency, the signal became clearer. Unfortunately, the signal was attenuated by almost a quarter, resulting in loss of much of the signal. Having a filter that has less than a decibel drop overall would prove to be beneficial in this scenario. Figures 33 and 34 show the signal across the ferrite bead with and without filtering. A proper signal is shown by run-stopping the oscilloscope. Although the image without the filtering looks clean, without utilizing the run-stop function, the signal contains noise that is significantly reduced through the filter.

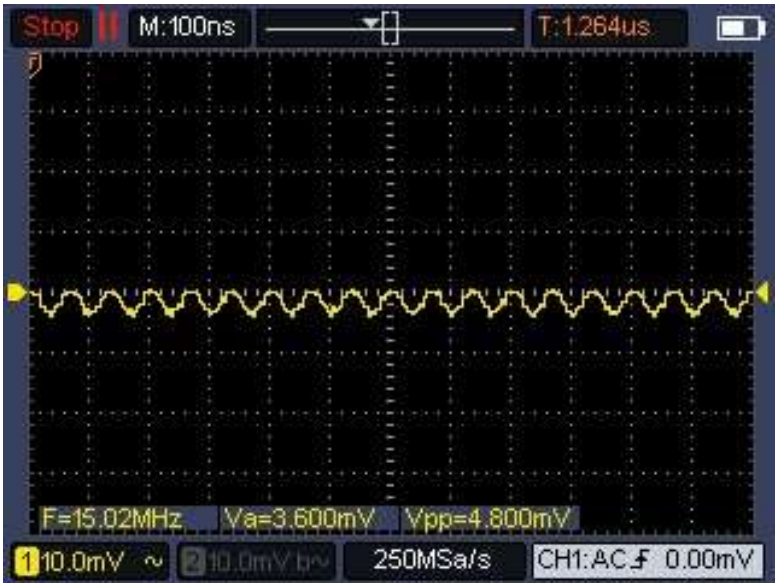

Figure 32. Approximate 4mV signal across ferrite bead without filtering.

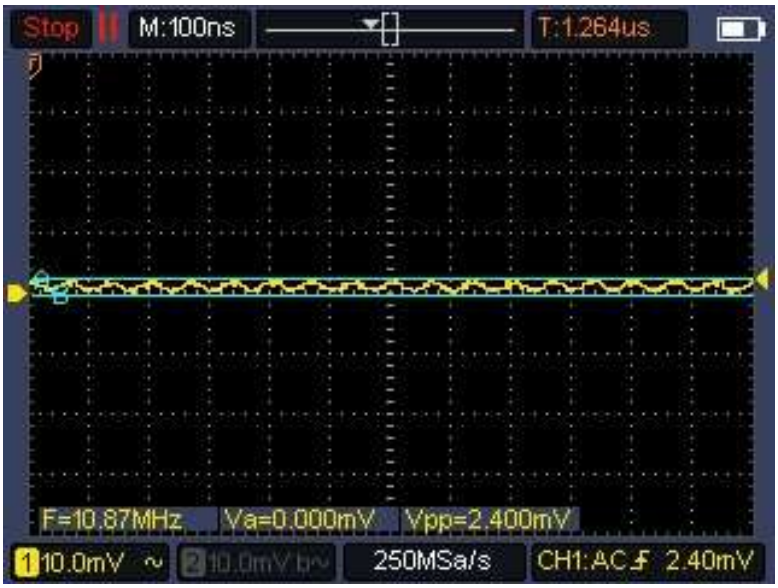

Figure 33. Attenuated signal with low-pass filtering.

6.2 Thermal Testing

Throughout the development of the GFCI prototype, maintaining equal resistance of the shunts under temperature changes was a constant concern which stemmed from the tendency of a resistor to change its resistance value based on temperature. If the values of the shunt resistors were unequal due to thermal drift, the voltage drops across them would not match, leading to erroneous tripping of the circuit breaker.

To investigate thermal differentials, an infrared camera [24] monitored shunt resistor temperatures during high power testing. Although the shunt resistors were not thermally bonded in this prototype, the temperature difference never exceeded ±0.56°C. This difference fell well within the accuracy of the thermal camera, specified by the datasheet as ± 3° C. Figure 35 shows the thermal behavior of the shunt resistors compared to the load resistors after two minutes. The shunt resistors were stable at 29°C, while the load resistors reached 63°C before the power was cut.

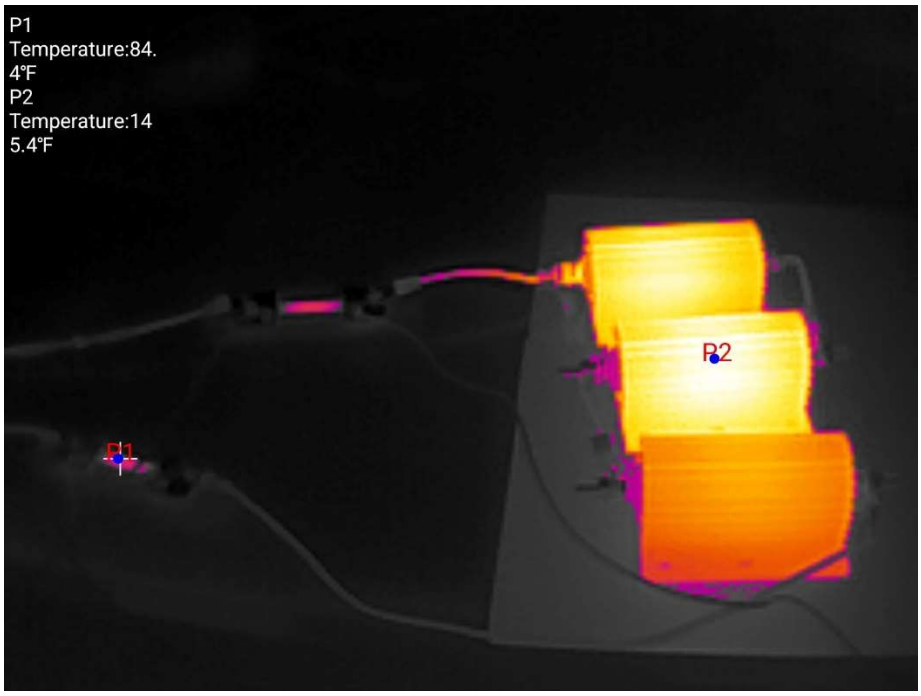

Figure 34. Temperature difference between shunt resistors and load resistors.

In another test performed with the IR camera, one of the shunt resistors was heated with a heat gun to intentionally create a temperature differential between the two shunt resistors. This test investigated the impact of thermal drift on the voltage drops across the shunt resistors to determine the minimum temperature difference that would cause a false trip. A 111.0°C temperature differential between the shunts yielded a 2mV voltage differential. This voltage differential is significantly less than what was expected, as this could be due to the tolerance of the temperature coefficient which would make these shunt resistors less affected by heat. When testing with the Arduino, this change in differential voltage was not sufficient to cause a trip. The results of these thermal tests are consistent with the simulations outlined in Section 5.1 Ground Fault Circuit Interrupter Schematic and Simulations.

7. Discussion

7.1 Meeting Objectives

After testing was performed on the final GFCI/AFCI prototype, the results were evaluated against the original design objectives defined in Chapter 3. This evaluation was based on how well the final testing results met the sponsor defined and team created project objectives. Throughout the project, the sponsor provided objectives took precedence over the team created objectives.

Sense 5mA Ground Fault Current with 20A Load Current

For the ground fault circuit interrupter design, the team successfully achieved the sponsor designated objective of detecting a minimum 5mA ground fault current amidst a 20A load current. To accomplish this, the GFCI design utilized precision amplifiers and low-pass filters to isolate and amplify the small ground fault signal, ensuring sensitivity and mitigating noise through careful calibration and tuning of circuit parameters. Through rigorous testing and validation, our system consistently demonstrated its capability to detect and respond to ground faults, thereby fulfilling one of the project's primary objectives. Also, in accordance with UL Standard 943, the system does not interrupt the circuit when the ground-fault current is less than 4mA [12].

Evaluate Thermal Behavior of Resistive Materials

Another sponsor-designated objective was to assess the impact of temperature variations on the shunt resistors and prevent any accidental trips due to temperature differences between them. Based on the thermal testing results outlined in Section 6.2, Thermal Testing, it was concluded that the shunt resistors we implemented have low temperature coefficients and are insensitive to differential temperatures. Consequently, thermal coupling of the shunt resistors is not required. However, for best practice, we recommend coupling the shunt resistors together using a series of vias on a PCB to minimize the potential for thermal drift, thereby reducing the risk of false trips. Figure 35 and Figure 36 illustrate the top and bottom sides of the PCB with the thermal coupling vias.

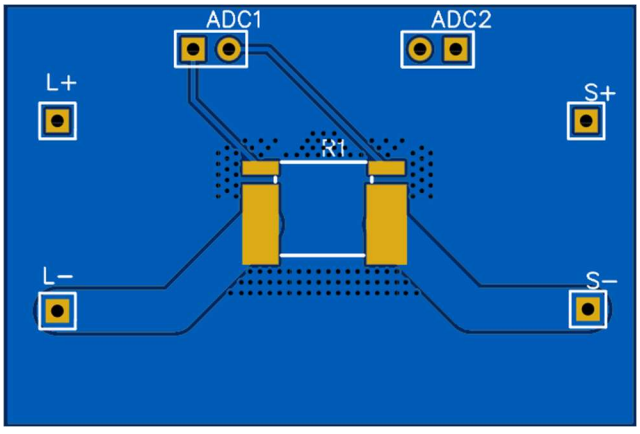

Figure 35. Top side of PCB with thermal coupling vias.

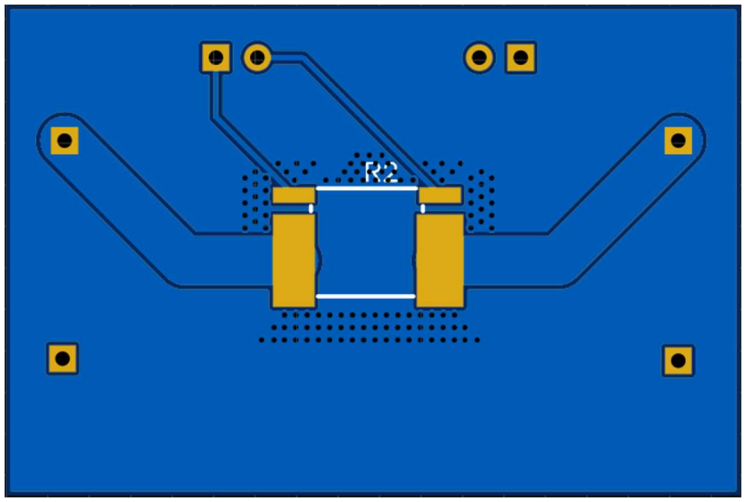

Figure 36. Bottom side of PCB with thermal coupling vias.

Follow UL Standard 943 for Trip Time

As per the results in Section 6.1 Higher Power Testing Results, the average response time of the GFCI breaker tripping ranged from 21.5575s to 38.515s. These results do not meet the project objective of following UL Standard 943 for the required trip time. According to Equation 1, introduced in Section 3, Problem Statement and Objectives, the required trip time for a 5mA fault current is 7.26s. As the fault current increases, the trip time decreases. Figure 37 shows the results of the timed trip testing and the required trip time for each of the fault currents that was tested.

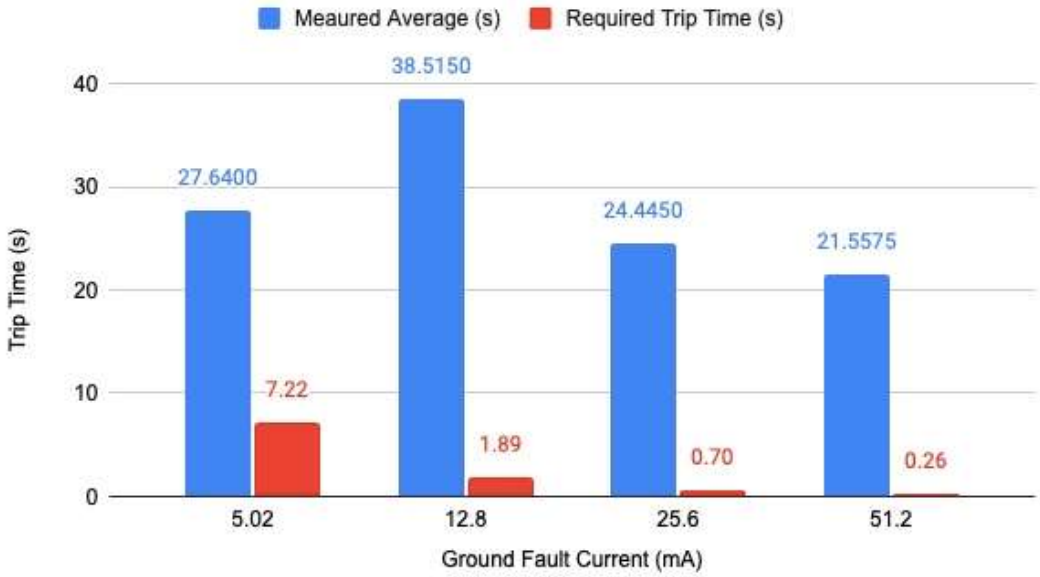

Figure 37. GFCI timed trip testing results.

The delayed trip time is due to the slow sample time of the Arduino, which only takes samples every 25ms. Since the readings are taken along the sine wave of the AC signal, it may require several cycles for the ADC to measure a difference between the two inputs, as the faults are only detectable when the voltage is near the 24V peak. When trials were unsuccessful and the trip did not occur within 90 seconds, the team suspects that the input signal was synchronized with the sampling time in such a way that the peak value was never measured.

To mitigate the time delay due to the slow sampling rate of the Arduino, two ADCs could be used to measure the differential voltages at the same instant. This would synchronize the readings and avoid the delay that the current prototype faces while waiting for a reading at the peak of the sinusoidal input signal.

Detect 100μA Signal in a Frequency Range of 10MHz to 20MHz

The sponsor required result from AFCI testing was defined as a detectable signal. A signal must be without excessive noise, consistent amplitude, and maintain frequency. Using the selected Tai-Tech Ferrite Bead in line with the load, before the GFCI detection resistors, a calibrated amplitude injection signal was induced. This high frequency injection of 100μA created a voltage drop of $4mV_{pk\text{-}pk}$ over the ferrite bead, indicating that the component is successfully creating an impedance at the designated frequency range at a magnitude that allows detection. From the oscilloscope, the signal is recognizable as a consistent 15MHz at $4mV_{pk\text{-}pk}$ with an acceptable level of noise.

When operating in an electrically noisy environment, high frequency noise over 20MHz may be detected over the ferrite bead. In this case, the low pass filter described in Section 4.7 could filter out high frequency noise with an approximate 1mV decrease in the resulting signal amplitude. With an effective microcontroller sampling rate, a differential amplifier would only detect a voltage drop at the specified time scale, ensuring that only desired frequency range voltage drops would create a breaker trip.

Decrease Cost and Size to Create a Competitive Product

Following the team's objective to create a competitive product in terms of both cost and size, the price of the sensing components from the current design was compared to the price for

the proposed dual shunt design. Table 8 summarizes the expected costs for sensing components for the current and proposed designs based on a DigiKey search.

Table 8. Cost comparison of current and proposed breaker sensing components.

Current Design			**Proposed Design**		
Component	Price	Quantity	Component	Price	Quantity
Inductive Coil [25]	$1.06-$13.30	2	2mΩ shunt resistors [26]	$0.56-$3.90	2
			Ferrite Bead [27]	$0.23	1
Total	$2.12-$26.60		Total	$1.35-$8.03	

Based on these calculations, the team succeeded in decreasing the cost of the standard dual function design. The cost of the amplification and filtering blocks was not included in this comparison because the current Schneider design also includes amplification and filtering.

One of the obvious benefits of transitioning from inductive coils to surface mount components as a sensing component is the size decrease. Figure 38 shows the relative size of the resistor and ferrite bead compared to the sensing coil. Although two shunts are required to replace the function of one coil, they are still significantly smaller and would decrease the volume of the sensing component by 96.7%. Additionally, the ferrite bead used for AFCI sensing is smaller than the AFCI sensing coil.

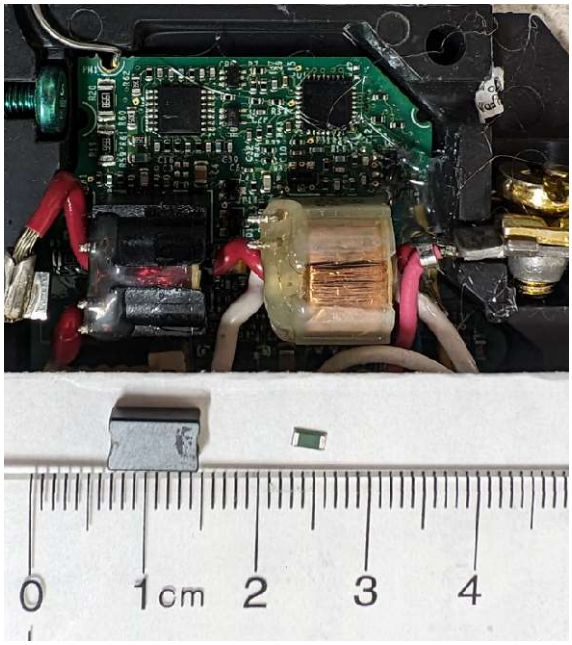

Figure 38. Close up of ferrite bead, SMD shunt resistor and the GFCI inductive coil.

7.2 Limitations

The team recognizes that not all the original project objectives were met and sought to identify the limitations of this research and provide potential solutions for future design iterations.

Tripping Efficacy

One of the limitations that arose while testing the higher power prototype was the inconsistent response of the GFCI circuitry and the failure to trip within 90 seconds. This behavior was only observed in a minority of the tests. The issue is suspected to be due to the microcontroller being unable to travel through the wave effectively as described in the discussion of the timed trip testing in Section 7.1. The solution to this problem would be to determine the optimal time for the microcontroller to effectively travel through the sine wave while minimizing the delay between measurements as the longer the delay between measurements causes detection to take longer.

Microcontroller Time Delay Reading AC Voltages

A primary limitation of the proposed design for the GFCI device is the time delay between the voltage measurements of the two ADC channels which leads to delays in the tripping time. The multiplexer within the ADS1115 IC communicates with the Arduino via the I2C communication bus, resulting in a delay of approximately 10ms. Although the ADC can read data in about 10µs, the communication delay of 10ms between readings leads to invalid data, as the measurements are taken at various times. To address this issue, it was determined that the microcontroller should wait until the next period before proceeding with data processing.

An alternative solution to mitigate this delay is to employ two separate microcontrollers and ADCs. This setup would enable synchronous ADC readings by both microcontrollers, allowing for accurate comparison and fault detection between the two channels.

Limited Load Diversity in Prototype Testing

During prototype testing, the load was limited to a purely resistive load, which does not adequately represent the variety of loads encountered in real-world scenarios. More realistic loads would include a combination of resistive, inductive, and capacitive elements. Testing with a motor could provide valuable insights as they introduce reactive power that results in phase shifts. These shifts may trigger false trips or prevent trips in the current prototype. Further testing would be necessary to evaluate the impact of larger phase shifts induced by reactive power on the current

prototype. Failure to detect and mitigate these phase shifts could result in false trips in practical applications.

Absence of a Tripping Mechanism

The goal of this project was to demonstrate the feasibility of the sensing circuits for ground and arc fault detection in circuit interrupter applications. A limitation of this project was the absence of a mechanism to interrupt power to the load upon fault detection. Instead, the prototype used an LED to symbolize when a signal would be sent to trip the breaker. The addition of a tripping mechanism in the prototype could be achieved using a relay to control when the load is powered on and off. The implementation would be straightforward and similar to controlling an LED with the Arduino's digital output pins. However, the decision to not include this feature in the prototype was driven by the need to focus on evaluating the performance of the sensing circuitry. Furthermore, the team recognized that our findings and concepts could be integrated into Schneider Electric's existing circuit interrupter mechanisms.

Power Consumption

The new shunt resistor design will have more power consumption than current Schneider Electric circuit breakers. The team assumed the signal processing components of the new design would be similar to the power consumption of the current electronic modules and that the shunts would add to this power consumption. In the Schneider Electric miniature circuit breakers product line, the electronic modules consume 800mW of power [30]. According to the higher power simulation, the shunt resistors will consume 373mW each. This is significant as it will add an additional 746mW of power dissipation, nearly doubling the total power consumption of the breakers.

7.3 Safety and Environmental Impact

Throughout this project, the team prioritized the well-being of the public and held "paramount the safety, health, and welfare of the public" in accordance with the Code of Ethics from the National Society of Professional Engineers [28]. Significant effort was dedicated to the design and testing of the product to ensure optimal functionality. The team also strived to adhere to relevant regulations such as minimum fault levels and tripping times. This ensures the design not only keeps the public safe but also contributes to the success of Schneider Electric.

Since GFCI and AFCI breakers are designed for electrical and fire safety, this prototype cannot be implemented unless it is fully tested and meets all standards for ground and arc fault circuit interrupters. Although the team has successfully met many of the objectives set forth at the beginning of the project, this design is intended only as a prototype for research purposes and should not be considered a reliable current interruption device.

In addition to the immediate safety concerns, it is essential to consider the long-term environmental impact of the device to identify potential pitfalls in the shunt resistor design that could lead to environmental harm. When evaluating the environmental impact of coils versus shunts, factors such as upstream material composition, ongoing energy usage, and downstream waste generation must be considered.

Both coils and resistors are made of various metals that require mining and processing that can negatively impact the environment such as habitat destruction, water and air pollution, and greenhouse gas emissions [29]. Since the shunts are significantly smaller than the coils, the proposed design is likely to have a smaller environmental impact due to material usage. In regard to ongoing energy usage, however, the shunt design will consume nearly twice as much power as a typical Schneider Electric breaker.

Another concern is the disposal process for coils compared to shunts. Both transformers and resistors may contain hazardous substances that require specialized handling and disposal procedures. However, both components can also be recycled to recover valuable materials like metals, thereby reducing the overall environmental impact. Proper disposal of circuit breakers involves disassembling them, separating the internal components, and bringing them to a recycling firm. Electronic waste contains hazardous materials that can be harmful to humans and the environment. Improper disposal of electronic waste, including circuit breakers, can lead to the release of hazardous materials into the environment. Heavy metals and harmful chemicals may contaminate soil, groundwater, and air, posing significant risks to human health, including organ damage and impacts on the nervous and reproductive systems [31].

Overall, the environmental impact of the shunt resistor circuit breaker design would be comparable to that of the coils. However, to identify any subtle differences that may compound during large scale manufacturing, a finalized product would need to be produced and assessed directly for comparison.

7.4 Manufacturability

When evaluating the current versus proposed solutions for a GFCI and AFCI circuit breaker, the current design uses a series of inductive coils to detect either arc faults or ground faults, as explained in Section 2.2 Current Solutions. This poses challenges in manufacturing, as these coils need to be made, tested, and, once installed, the correct number of wires must be run through the center of these coils. For ground fault detection, the load and line wires run through the coil, while for arc fault detection, only one wire, typically the load wire, needs to run through the coil. This process of having to feed a wire through these pick-up coils can slow down production, as it is not as fast as standard surface mount assembly. In contrast, the assembly of the researched prototype would be simpler and more efficient as it would rely only on surface mount assembly. One potential downside with this proposed design is that if thermal bonding is required, the PCB would need to be double sided to minimize the thermal differential between the two shunt resistors. However, assembly of the proposed design would be simpler and decrease specialized construction compared to the current design.

Another comparison to consider between the current versus proposed solutions is the cost of sensing components. As described in Section 7.1 Meeting Objectives, the price of the sensing components in the dual shunt design is estimated to be lower than that of the current design. Finally, the calibration procedure detailed in Section 4.4 Ground Fault Circuit Interrupter Signal Processing adds to the ease of manufacturing of the proposed device because the calibration removes the need for precision resistors or resistor matching in the GFCI amplification stage. In terms of both component costs and manufacturing costs, the proposed design would be less expensive for the manufacturer.

Conclusion

This project has successfully explored alternatives to traditional inductive coils for circuit interrupter devices. By replacing the coils with resistive shunts and a ferrite bead, the team made progress towards detecting both ground and arc faults. With this prototype, the team aimed to address issues related to size, cost, and susceptibility to non-standard electrical noise.

The ground fault circuitry, utilizing the shunt resistors, can accurately detect a 5mA ground fault current amidst a 20A load current and send a signal to trip a breaker. The arc fault circuitry,

utilizing the ferrite bead, can effectively produce a small voltage signal when a 15MHz 100µA signal is injected that, with future development, can be used to trip a breaker. The team also met other objectives including evaluating the thermal behavior of resistive materials and reducing cost and size for a competitive product.

Despite these achievements, several limitations of the prototype were identified including a delayed response time for tripping, limited load diversity during testing, and absence of a tripping mechanism. Addressing these limitations would be crucial for further development. For future research, we propose modifications for a 120V-compatible circuit interrupter, microcontroller improvements, and the development of a PCB. Overall, this project lays the groundwork for future research in circuit interrupter designs using coil alternatives.

8. Recommendations for Future Testing

8.1 120V Research

To function effectively as a product, this GFCI/AFCI breaker must be compatible with standard 120VAC wall power. The main challenge that arises when using a higher input voltage is that it exceeds the common mode input voltage of the INA145 difference amplifier. The common mode voltage of the 24V/20A setup fell slightly within the bounds of the common mode voltage specified by the INA145 datasheet as -30V to 28V [17]. A 120V source voltage results in a common mode voltage that is approximately 120V, given the negligible voltage drop across each shunt in comparison to the large input voltage. Rather than tying a 120VDC source to the V_{ref} pin of the INA145 to offset its common mode voltage limit, the team recommends utilizing the AD8479 difference amplifier for higher power applications. This amplifier has a ±600V common mode voltage range and can operate with the same ±15V power supply as the INA145 [32]. Unlike the INA145 difference amplifier, however, the AD8479 has a fixed gain of 1, so the gain of the LM741 amplifier must be increased to compensate.

To simulate the 120VAC setup, an 8Ω load was selected to draw 15A, the standard current limit of 120V outlets. With a 15A current across a 1.875mΩ shunt resistor, a 28.125mV voltage differential is generated across the shunt, which is amplified to approximately $3V_{pk\text{-}pk}$ by setting the gain of the LM741 amplifier to 41. The full GFCI schematic is shown in Figure 39 below. The fault load resistor is 24kΩ to draw a fault current of 5mA.

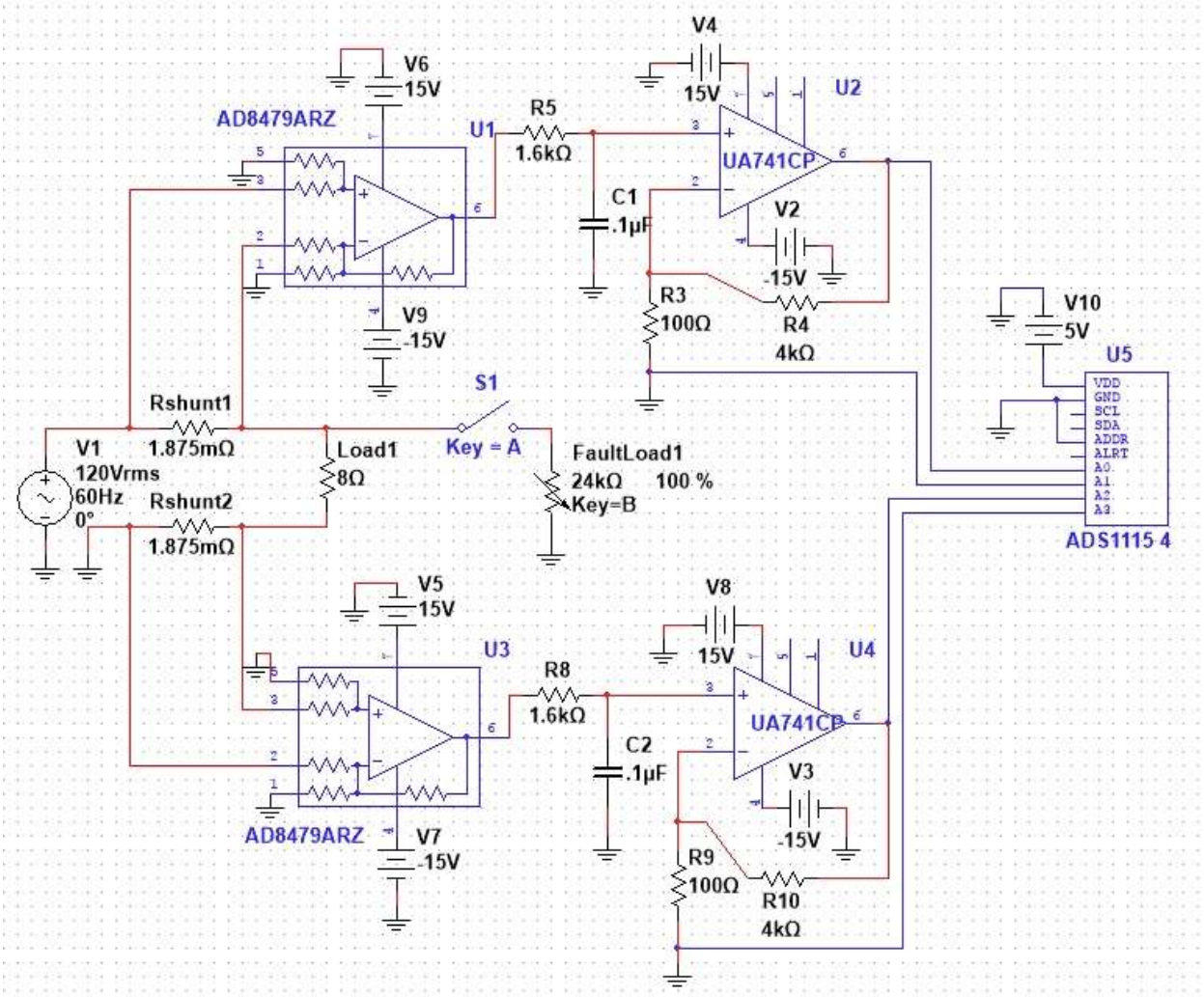

Figure 39. GFCI schematic for 120V/15A setup

The differential output voltage of the shunts was measured under normal and fault conditions to determine whether a 5mA ground fault would be detectable. Under normal conditions, the peak differential output voltage was 220.9804mV. After closing S1 to simulate a fault, the peak differential output voltage was 221.5226mV. Based on these results, the output voltage is expected to change by 542µV, well within the 125µV minimum measurable step of the ADS1115. The differential output signal before and after the fault occurred is shown in Figure 40.

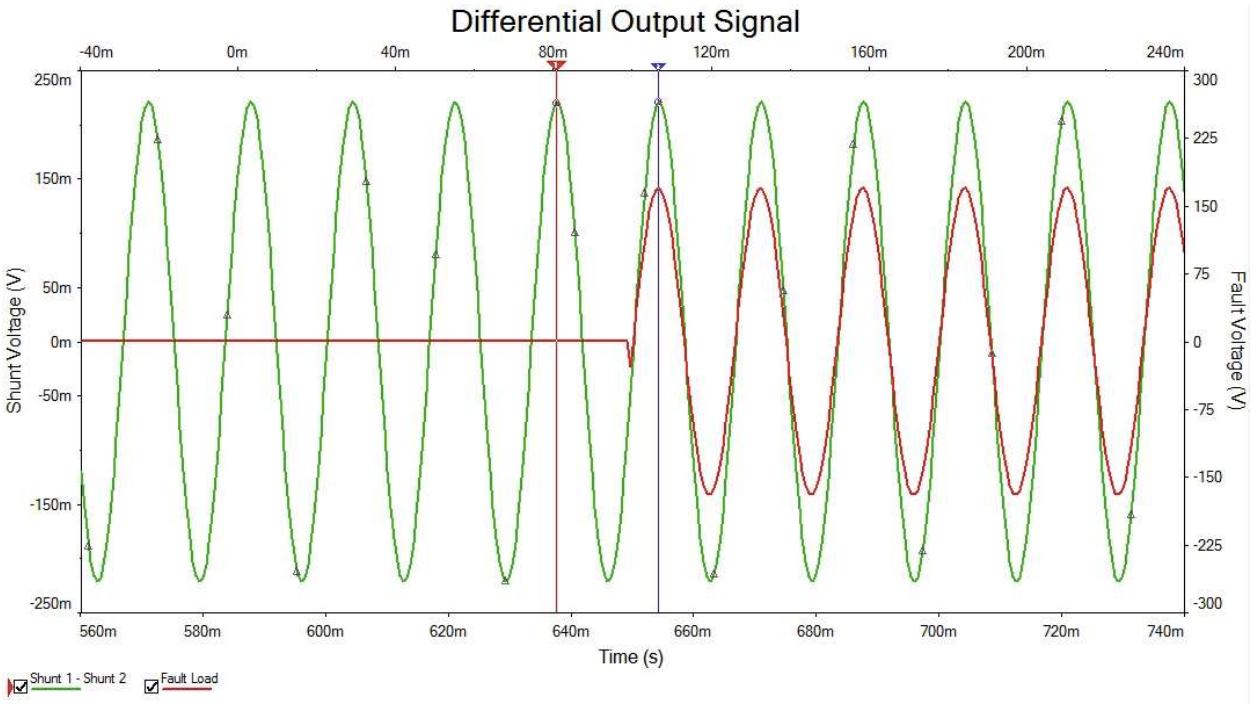

Figure 40. Differential voltage signal before and after ground fault, 120VAC setup

Based on this simulation, the device developed by the team can be easily scaled to function with standard 120VAC wall power.

8.2 Microcontroller Improvement

To detect the AFCI representation signal, an improved microcontroller would have to be incorporated into the design. Due to the Nyquist sampling theorem, for the 10-20MHz digital signal to be processed, the clock speed must be at least twice the sampling rate. Therefore, a microcontroller with a clock speed of at least 40MHz will be required, a significant increase over the Arduino's 16MHz clock speed. Schneider Electric currently uses a microcontroller with a clock speed of 32MHz, able to read most of the frequency range. Alternative microcontrollers in similar product lines are available with sufficiently high clock speeds at comparable prices. The frequency of the input signal could also be reduced using a mixer or detector circuit such that direct sampling of the signal would not be necessary, and a lower sampling rate could be used. In addition to this, analog input resolution could be improved. The current ADC can read at ~125µV per step, but it may be desirable for an improved microcontroller to read directly from the ferrite bead, as it would have enough resolution to read the fault.

8.3 Creating a Printed Circuit Board

Given additional time, the team would have pursued the development of a printed circuit board (PCB) that would integrate both GFCI and AFCI circuitry. This PCB prototype would resemble what would go inside the final breaker assembly intended for production by Schneider Electric. Such a PCB would allow for the assessment of component functionality within the printed environment that would be used in production. Specifically, the team would recommend an evaluation into the effect of temperature on the circuit's performance to determine the effectiveness of thermal coupling. The PCB would also remove long wire connections and the potential for accidental shorts during testing. While it would remove noise from long wire connections, an analysis of the potential introduction of new noise sources within the PCB would have to be done. The PCB layout could be created utilizing either MultiSim or LTspice tools from the completed simulation circuits that include the specific components used in the breadboard assembly. Overall, a PCB would allow for a compact design and improved testing reliability and consistency.

Appendices

Appendix A. Abbreviations

ADC – Analog to Digital Converter

AFCI – Arc Fault Circuit Interrupter

GFCI – Ground Fault Circuit Interrupter

IC – Integrated Circuit

IR – Infrared Camera

LED – Light Emitting Diode

LPF – Low Pass Filter

PCB – Printed Circuit Board

SMD – Surface Mount Device

Appendix B. LTspice GFCI Schematic and Simulation

Below in Figure 41 is the schematic of the higher power test setup in LTspice. The symbols of the operational amplifiers were imported from the manufacturers' websites and converted to be compatible with LTspice. The colored arrows correspond to the probed signals of the transient sweeps in Figures 42 and 43. The transient sweeps show the voltage across the shunt, the voltage at the differential amplifier output, and the voltage at the low pass filter when a fault is not occurring. The voltages across both shunts were 37mV; the voltages at the differential amplifier outputs were 328mV; and the voltages at the low pass filters were 985mV.

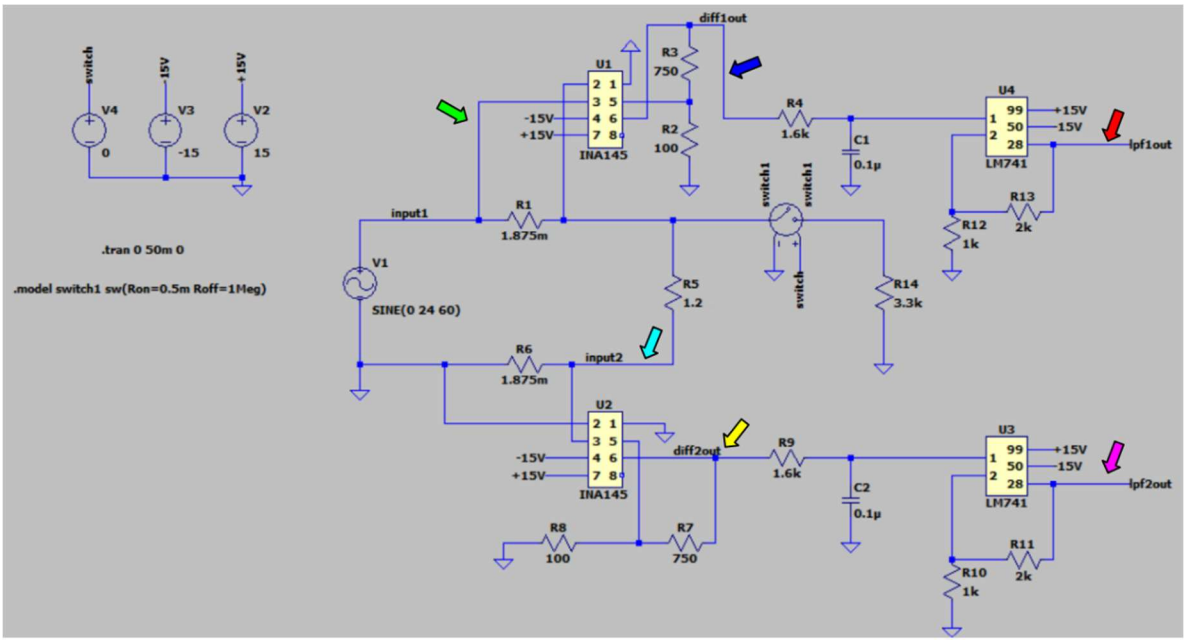

Figure 41. Combined GFCI and AFCI schematic in LTspice.

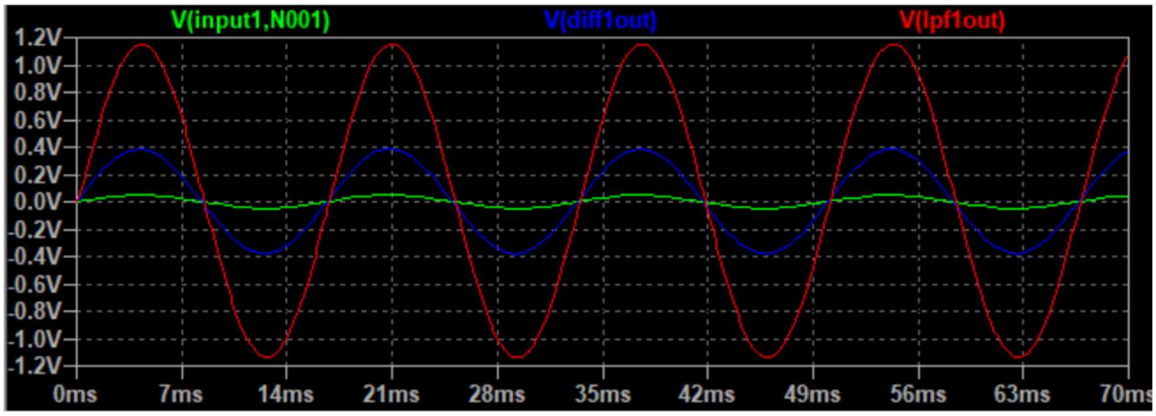

Figure 42. Transient sweep results of shunt 1 circuitry.

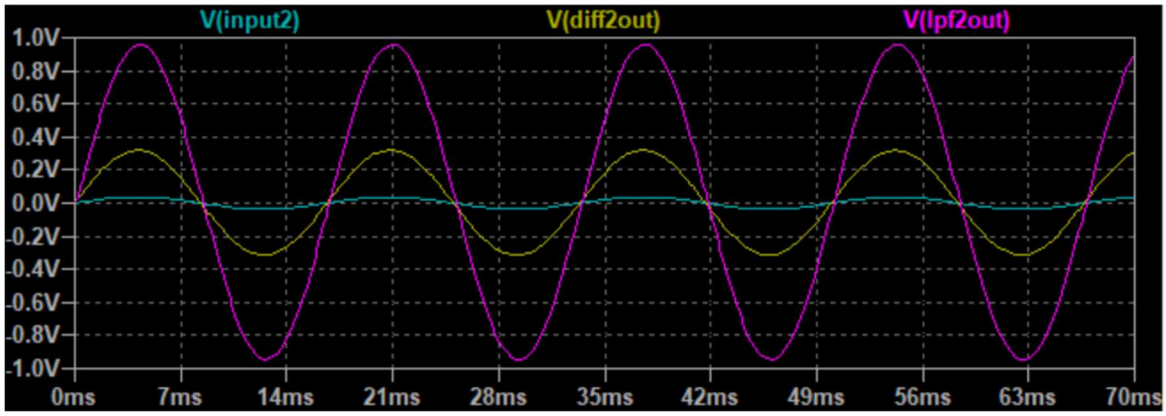

Figure 43. Transient sweep results of shunt 2 circuitry.

Appendix C. Ground Fault Detection Arduino Code

```
#include <Adafruit_ADS1X15.h>

#include <Adafruit_ADS1X15.h>

Adafruit_ADS1115 ads;  /* Use this for the 16-bit version */
//Adafruit_ADS1015 ads;     /* Use this for the 12-bit version */

constexpr int READY_PIN = 3;
int i = 0;
int j = 0;
int k = 0;
int maxValue;
int newValue;
int tripValue;

#ifndef IRAM_ATTR
#define IRAM_ATTR
#endif

volatile bool new_data = true;
void IRAM_ATTR NewDataReadyISR() {
  new_data = true;
}


void setup(void) //Initializing the arduino to communicate with the serial
monitor, and printing some important messages
{
  Serial.begin(9600);
  Serial.println("GFCI Testing");
  Serial.println("Reading Differential Voltages Between A0, A1 and A2, A3");
  Serial.println("Running Auto Calibration");
  pinMode(4, OUTPUT);
  digitalWrite(4, LOW); //Ensures LED on pin 13 will be off
  delay(1000);

  if (!ads.begin()) {
    Serial.println("Failed to initialize ADS.");
    while (1);
  }

  pinMode(READY_PIN, INPUT);
  attachInterrupt(digitalPinToInterrupt(READY_PIN), NewDataReadyISR, FALLING);
```

```
}


void loop(void) //Primary Code
{
  for(j; j < 1000; j++){ //This is the auto calibration code it runs 1000 times
and its job is to find the max step value when no GFCI is occurring

  ads.startADCReading(ADS1X15_REG_CONFIG_MUX_DIFF_2_3, false); //Reads ADC Value

  delay(15.2); //Since the ADC is slower than expected we cannot read a voltage
value immediately after due to multiplexer taking time to work, this delay is to
skip forward one period of 60 Hz

  int16_t results1 = ads.getLastConversionResults(); //Assigns Results1 from ADC
diff 2 & 3

  //Serial.print("Differential1: "); Serial.print(results1); Serial.print("(");
Serial.print(ads.computeVolts(results1)); Serial.println("mV"); //Used for
debugging

  ads.startADCReading(ADS1X15_REG_CONFIG_MUX_DIFF_0_1, false); //Reads ADC Value

  delay(12); //This delay is to help us move throughout the sine wave so we do
not just sit and read one voltage value

  int16_t results0 = ads.getLastConversionResults(); //Assigns results0 from ADC
diff 0 & 1

  //Serial.print("Differential0: "); Serial.print(results0); Serial.print("(");
Serial.print(ads.computeVolts(results0)); Serial.println("mV"); //Used for
debugging

  int16_t adcDiff = abs(abs(results0 - results1) - 0); //Finds the difference
between ADC

  newValue = adcDiff; //for finding max value

  if(newValue > maxValue){ //Determins if new value is greater than max value
    maxValue = newValue; //If new value is greater than current max value, it
assigns new value to max value
  }
  else{
  }
```

```
  tripValue = maxValue + 1; //Sets trip value 3 steps higher than calibration
value
  Serial.print("Trip Value = "); Serial.println(tripValue); //Print debugging
  } //End of autocalibration

  if(k == 0){ //Just shows that autocalibration is complete
    Serial.println("Auto Calibration Complete");
    delay(1000);
    k = 1;
  }


  ads.startADCReading(ADS1X15_REG_CONFIG_MUX_DIFF_2_3, false); //Reads ADC value

  delay(15.2); //Since the ADC is slower than expected we cannot read a voltage
value immediately after due to multiplexer taking time to work, this delay is to
skip forward one period of 60 Hz

  int16_t results1 = ads.getLastConversionResults(); //sets results1 equal to ADC
diff 2 & 3

  //Serial.print("Differential1: "); Serial.print(results1); Serial.print("(");
Serial.print(ads.computeVolts(results1)); Serial.println("mV"); //For debugging

  ads.startADCReading(ADS1X15_REG_CONFIG_MUX_DIFF_0_1, false); //Reads ADC Value

  delay(12.5); //Allows us to travel throughout the sine wave so we arent stuck
at one voltage value

  int16_t results0 = ads.getLastConversionResults(); //sets results0 equal to ADC
diff 0 & 1

  //Serial.print("Differential0: "); Serial.print(results0); Serial.print("(");
Serial.print(ads.computeVolts(results0)); Serial.println("mV"); //Used for
debugging

  int16_t adcDiff = abs(abs(results0 - results1)); //Finds differential voltage
values between ADC readings

  newValue = adcDiff; //assigns ADC differential to new value, which is used for
finding the max value
  //Serial.println(newValue);

  if(newValue > maxValue){ //Used for finding the max value of the ADC step
    maxValue = newValue;
```

```
  }
  else{
  }

  Serial.print("ADC Differential = "); Serial.println(maxValue); //Used for
debugging and showing off values

  if(maxValue >= tripValue){  //Determines if the difference between the shunt
resistors is enough to trip the breaker, 100 was just an arbitrary number
    digitalWrite(4, HIGH);  //turns on LED on pin 4
    Serial.println("BREAKER TRIPPED");
    Serial.println("Power Cycle to Reset");
    while(1); //Locks Arduino in loop until power cycle
  }

  else{
      digitalWrite(4, LOW); //Turns off LED on pin 13
  }
}
```

Appendix D. Arc Fault Detection Arduino Code

```
#include <Adafruit_ADS1X15.h>

#include <Adafruit_ADS1X15.h>

Adafruit_ADS1115 ads;  /* Use this for the 16-bit version */
//Adafruit_ADS1015 ads;     /* Use this for the 12-bit version */

constexpr int READY_PIN = 3;

#ifndef IRAM_ATTR
#define IRAM_ATTR
#endif

volatile bool new_data = true;
void IRAM_ATTR NewDataReadyISR() {
  new_data = true;
}

void setup(void)
{
  Serial.begin(9600);
  Serial.println("AFCI Testing");

  Serial.println("Reading Differential Voltage Between A0 and A1");
```

```
  digitalWrite(13, LOW); //Ensures LED on pin 13 will be off

  if (!ads.begin()) {
    Serial.println("Failed to initialize ADS.");
    while (1);
  }

  pinMode(READY_PIN, INPUT);
  attachInterrupt(digitalPinToInterrupt(READY_PIN), NewDataReadyISR, FALLING);

}
void loop(void)
{

  ads.startADCReading(ADS1X15_REG_CONFIG_MUX_DIFF_0_1, false);

  delay(10);

  int16_t results = abs(ads.getLastConversionResults());

  Serial.print("Differential: "); Serial.println(results); //Serial.print("(");
Serial.print(ads.computeVolts(results)); Serial.println("mV)");

    if(results >= 200){  //Determines if the difference between the shunt
resistors is enough to trip the breaker, 100 was just an arbitrary number
    digitalWrite(13, HIGH);  //turns on LED on pin 13
    Serial.println("BREAKER TRIPPED");
    Serial.println("Power Cycle to Reset");
    //delay(5000);  //1 Second Delay
    while(1);
  }

  else{
      digitalWrite(13, LOW); //Turns off LED on pin 13
  }

  delay(1000);
}
```

References

[1] W. Delsman, “Guide to Ground Fault Sensing - IAEI Magazine,” May 01, 2020. https://iaeimagazine.org/issue/may-june-2020/guide-to-ground-fault-sensing/ (accessed Sep. 04, 2023).

[2] Fluke, “Troubleshooting power harmonics: Basic troubleshooting using multimeters and current clamps,” Fluke, https://www.fluke.com/en-us/learn/blog/power-quality/troubleshooting-power-harmonics (accessed Oct. 25, 2023).

[3] R. C. Quick, “Ground Fault Circuit Interrupter—Design and Operating Characteristics,” *IEEE Transactions on Industry Applications*, vol. IA-11, no. 1, pp. 50–55, Jan. 1975, doi: 10.1109/TIA.1975.349257.

[4] “American Circuit Breaker Manufacturers Association.” https://acbma.org/resources.html (accessed Sep. 04, 2023).

[5] “Using Advanced Technology to Reduce Electrical Fires,” AFCI Safety, https://www.afcisafety.org/wp-content/uploads/2020/10/AFCIs-Using-Advanced-Technology-to-Reduce-Electrical-Fires.pdf (accessed Sep. 4, 2023).

[6] G. D. Gregory, K. Wong, and R. F. Dvorak, “More about arc-fault circuit interrupters,” *IEEE Transactions on Industry Applications*, vol. 40, no. 4, pp. 1006–1011, Jul. 2004, doi: 10.1109/TIA.2004.831287.

[7] “The history of Square D.” Accessed: Oct. 24, 2023. [Online]. Available: https://www.se.com/ww/en/about-us/company-profile/history/square-d.jsp

[8] “Square D | Encyclopedia.com.” Accessed: Oct. 24, 2023. [Online]. Available: https://www.encyclopedia.com/books/politics-and-business-magazines/square-d

[9] D. A. Lee, A. M. Trotta, and W. H. King, “New Technology for Preventing Residential Electrical Fires: Arc-Fault Circuit Interrupters (AFCIs),” *Fire Technology*, vol. 36, no. 3, pp. 145–162, Aug. 2000, doi: 10.1023/A:1015410726786.

[10] A. Software, “Thermal Circuit Breakers,” *Fuses Unlimited*. https://www.fusesunlimited.com/products/thermalcircuitbreakers#:~:text=In%20a%20thermal%20circuit%20breaker,rates%20as%20the%20temperature%20rises. (accessed Feb. 13, 2024).

[11] “What is a Circuit Breaker & How Does it Work?,” *RSP Supply*. https://rspsupply.com/education/a-23-what-is-a-circuit-breaker/ (accessed Feb. 13, 2024).

[12] UL, "UL Standard for Safety for Ground-Fault Circuit-Interrupters, UL 943," 4th ed., Feb. 1, 2006.

[13] UL, "Arc-Fault Circuit Interrupters (AFCIs) – Type and Performance Considerations," https://code-authorities.ul.com/wp-content/uploads/2014/05/Dini2.pdf (accessed Mar. 20, 2024).

[14] “Shunt Resistor | Resistor Applications | Resistor Guide.” Accessed: Feb. 20, 2024. [Online]. Available: https://eepower.com/resistor-guide/resistor-applications/shunt-resistor/

[15] “Resistor materials | Resistor Guide,” *eepower.com*. https://eepower.com/resistor-guide/resistor-materials/#

[16] C. Udegbue, “Current sensing with different types of amplifiers: Video,” Current sensing with different types of amplifiers | Video | TI.com, https://www.ti.com/video/6076312538001 (accessed Sep. 6, 2023).

[17] Texas Instruments, “Programmable Gain Difference Amplifier,” INA145 datasheet, Sept. 2023.

[18] “IA0515S,” Digi-Key Electronics. Accessed: Mar. 01, 2024. [Online]. Available: https://www.digikey.com/en/products/detail/xp-power/IA0515S/4487732

[19] “LM741 data sheet, product information and support | TI.com.” Accessed: Mar. 01, 2024. [Online]. Available: https://www.ti.com/product/LM741

[20] “Active Low-pass Filter,” Basic Electronics Tutorials, https://www.electronics-tutorials.ws/filter/filter_5.html (accessed Jan. 29, 2024).

[21] “Half-wave rectifier,” Half-Wave Rectifier | Analog Devices, https://www.analog.com/en/resources/glossary/half-wave-rectifier.html (accessed Feb. 2, 2024).

[22] Electronics tutorials, “Series Resonance in a Series RLC Resonant Circuit,” Basic Electronics Tutorials, Jun. 04, 2018. https://www.electronics-tutorials.ws/accircuits/series-resonance.html

[23]“Parallel Resonance and Parallel RLC Resonant Circuit,” Basic Electronics Tutorials, Oct. 15, 2018. https://www.electronics-tutorials.ws/accircuits/parallel-resonance.html

[24] “InfiRay Xtherm II T2 Search - thermal imaging camera for smart phones: outdoor observation & hunting, IR 256x192,” https://www.vovov.hu/en/spd/iray-t2se/InfiRay-Xtherm-II-T2-Search-thermal-imaging-camera#page_artdet_tabs (accessed Feb. 12, 2024).

[25] “Fixed Inductors | Electronic Components Distributor DigiKey.” Accessed: Feb. 26, 2024.

[Online]. Available: https://www.digikey.com/en/products/filter/fixed-inductors/71?s=N4IgjCBcoGwJxVAYygMwIYBsDOBTANCAPZQDaIALAAxwDMdIAuoQA4AuUIAymwE4CWAOwDmIAL5jCAJjIg2RXkX4ATLAAIkSzE0IBWRCBZQwrI5Cm7JIGAZWcAtGCpUQrDpBCu5ATxa5O6NgoEkA

[26] "Resistors | Chip Resistor - Surface Mount," Digi-Key Electronics. Accessed: Feb. 26, 2024. [Online]. Available: https://www.digikey.com/en/products/filter/chip-resistor-surface-mount/52

[27] "BPH 853025R5-101T," Digi-Key Electronics. Accessed: Feb. 26, 2024. [Online]. Available: https://www.digikey.com/en/products/detail/tai-tech-advanced-electronics-co-ltd/BPH-853025R5-101T/17835579

[28] "Code of ethics," Code of Ethics | National Society of Professional Engineers, https://www.nspe.org/resources/ethics/code-ethics (accessed Sep. 21, 2023).

[29] "How can metal mining impact the environment?," American Geosciences Institute, https://www.americangeosciences.org/critical-issues/faq/how-can-metal-mining-impact-environment (accessed Feb. 25, 2024).

[30] "What is the power consumption of the circuit boards in the QO and Hom GFI, CAFI, and DF circuit breakers?: Schneider Electric USA," www.se.com, https://www.se.com/us/en/faqs/FA122790/ (accessed Mar. 12, 2024).

[31] Beanstalk, "Recycling Electrical Breakers and other equipment," Cycling, https://www.cjdecycling.com/recycling-electrical-breakers/ (accessed Oct. 2, 2023).

[32] "AD8479 Datasheet and Product Info | Analog Devices." Accessed: Feb. 28, 2024. [Online]. Available: https://www.analog.com/en/products/ad8479.html

[33] "What to do if you were exposed to covid-19," Centers for Disease Control and Prevention, https://www.cdc.gov/coronavirus/2019-ncov/your-health/if-you-were-exposed.html (accessed Sep. 21, 2023).

[34] S. J. Bitar, "Electrical Safety," in ECE 2799 Electrical & Computer Engineering Design, Apr. 2022

[35] W. Storr, "Differential Amplifier," Basic Electronics Tutorials, https://www.electronics-tutorials.ws/opamp/opamp_5.html (accessed Feb. 12, 2024).

[36] M. Jasica, "High Voltage Safety," Safety, https://safety.ep.wisc.edu/hazards/high-voltage-safety (accessed Sep. 19, 2023).

[37] “Isolation Transformers,” Industrial Quick Search Directory, https://www.iqsdirectory.com/articles/electric-transformer/isolation-transformers.html (accessed Oct. 4, 2023).

[38] P. Reid, RE: Questions and Bill of Materials, Oct. 9, 2023

[39] P. Reid, Personal Communication, Feb. 7, 2024